Life Sciences 379 (2025) 123837

Contents lists available at ScienceDirect

Life Sciences

journal homepage: www.elsevier.com/locate/lifescie

Human osteosarcoma cell secretome impairs neonatal mouse calvarial osteogenic cells functions and modifies the nanoparticles-derived protein profile

Argia Ucci [a], Luca Giacchi [a], Maria Concetta Cufaro [b,c], Chiara Puri [a], Michela Ciocca [a], Fabio Di Ferdinando [b,c], Piero Del Boccio [c,d], Alfredo Cappariello [e,*], Nadia Rucci [a]

[a] Department of Biotechnological and Applied Clinical Sciences, University of L'Aquila, L'Aquila, Italy
[b] Department of Innovative Technologies in Medicine and Dentistry, "G. d'Annunzio" University of Chieti-Pescara, Italy
[c] Centre of Advanced Studies and Technology (CAST), "G. d'Annunzio" University of Chieti-Pescara, Italy
[d] Department of Pharmacy, "G. d'Annunzio" University of Chieti-Pescara, Italy
[e] Department of Life, Health and Environmental Sciences, University of L'Aquila, L'Aquila, Italy

ARTICLE INFO

Keywords:
Bone matrix
Nanoparticles
Osteosarcoma
Osteoblast
Proteome

ABSTRACT

Osteosarcoma is the most common pediatric primary bone tumor, whose growth strictly relies on a complex interplay among tumor cells, resident cells, and the bone matrix. We investigated the effects of secretome collected from the human osteosarcoma cell line MNNG/HOS on mouse primary osteogenic cells, finding that prolonged exposure alters osteoblast phenotype and activity. MNNG/HOS secretome also reduces the production and release of collagen type I, the most abundant constituent of the bone matrix, and hinders osteoblast ability to form nodule of mineralization, compared to osteogenic cells treated with their own secretome. Given the crucial role exerted by secretome on tumor growth, we aimed also to determine whether osteosarcoma cells secretome can influence the osteoblast release of extracellular nanoparticles (NPs) as well as NPs protein cargo. Intriguingly, we found that MNNG/HOS secretome exerts a direct effect on osteoblast-NPs, reprogramming their protein cargo and subsequently influencing extracellular matrix composition and collagen formation, in favor of tumor progression. Overall, our findings indicate the ability of MNNG/HOS cells to fuel their own malignancy by deranging bone matrix composition and stimulating osteoblast-nanoparticles shuttling of osteosarcoma promoting factors.

1. Introduction

Although rare, osteosarcoma is unfortunately the most prevalent malignant bone tumor, occurring in adolescents and young adults [1,2]. The common sites of tumor formation are those with the most extensive longitudinal bone growth, such as distal femur, proximal tibia and proximal humerus [3]. To date, treatment strategies include surgical resection combined with adjuvant chemotherapy [3]; however, osteosarcoma is still characterized by a poor prognosis due to its high aggressiveness, eventually leading to metastasis development, with the lung being the preferential affected organ [4].

Osteosarcoma derives from a malignant transformation of mesenchymal stem cells (MSCs) and is characterized by deposition of an osteoid-like matrix, with varying degrees of mineralization [5]. This osteoid matrix in turn enables a supportive scaffold for tumor progression [6]. Indeed, osteosarcoma cells grow in a complex and dynamic microenvironment, the bone matrix, in which they interact with different types of resident cells, like osteoblasts, osteoclasts, osteocytes, MSCs, endothelial and immune cells. This interplay has a crucial role in tumor progression and invasion [5]. Moreover, the extracellular matrix includes several components such as collagens, fibronectin, osteopontin, bone sialoprotein (BSP) II and γ-carboxyglutamic acid (GLA) proteins, whose deregulation contributes to aberrant signaling, eventually promoting osteosarcoma growth [6]. As an example, it has been demonstrated that matrix-Gla protein (MGP) overexpression in osteosarcoma cells increases lung metastases in an orthotopic mouse model, by a mechanism involving metalloproteinase activity and TGFβ-induced Smad2/3 phosphorylation [7]. Fibronectin is an adhesion protein highly

* Corresponding author.
E-mail address: alfredo.cappariello@univaq.it (A. Cappariello).

https://doi.org/10.1016/j.lfs.2025.123837
Received 30 October 2024; Received in revised form 22 June 2025; Accepted 1 July 2025
Available online 9 July 2025

expressed in the bone matrix, which is able to interact with collagen, and a significantly higher expression of this glycoprotein has been found in resistant osteosarcoma cell lines [8].

The intercellular crosstalk is a crucial process for the physiological and pathological tissue homeostasis, mediated by different cellular strategies such as the release of the secretome, a complex cellular product composed by soluble and extracellular vesicles (EVs) bound molecules, such as proteins, lipids and nucleic acid [9]. With regard to the interplay between bone cells and osteosarcoma cells, we recently demonstrated a bidirectional crosstalk by means of EVs as mediators [10,11]. In particular, we found that treatment of bone cells with osteosarcoma cells-derived EVs promotes a series of anti-osteoblastogenic, pro-inflammatory and pro-angiogenic effects, eventually contributing to the tumor expansion [10]. Likewise, we also demonstrated that osteoblast-derived EVs reduced osteosarcoma cells' aggressiveness and viability through redox-dependent signaling pathways [11].

Based on the above background, in this work we aimed at investigating how osteosarcoma cells-secretome alters osteoblast homeostasis and interferes with its autocrine regulation. Given the crucial role exerted by extracellular nanoparticles in the crosstalk between bone cells and tumor cells, our goal was also to determine whether osteosarcoma cells secretome is able to influence the release of osteoblast-nanoparticles as well as the nanoparticles protein profile, the latter assessed by proteomics approach through nano liquid chromatographic coupled tandem mass spectrometry (nanoLC-MS/MS). Our finding demonstrated that osteogenic cells educated by osteosarcoma cell secretome show an impaired ability to release collagen I and mineralize; moreover, osteosarcoma cell secretome is able to change the profile of osteoblast-derived nanoparticles towards a phenotype that could promote their growth.

2. Materials and methods

2.1. Materials

Dulbecco's modified Minimum Essential Medium (DMEM), Fetal Bovine Serum (FBS), penicillin, streptomycin and trypsin were from GIBCO (Uxbridge, UK). Sterile plasticware was from Falcon Becton-Dickinson (Cowley, Oxford, UK), Costar (Cambridge, MA, USA) or Euroclone (Milan, Italy). The anti-Annexin II (cat #sc-9061), -Matrilin-4 (cat #sc-374652), -CD81 (cat #sc-166029) and β-Actin (cat #sc-81178) antibodies were from Santa Cruz Biotechnology Inc. (Santa Cruz, CA, USA); the anti-CD63 antibody (cat #PA5-92370) was from Thermo Fisher Scientific (Waltham, MA, USA); the anti-Collagen type I (cat #AB-82138) was from Immunological Sciences (Rome, Italy). The Super-Signal Chemiluminescent substrate was from Thermo Scientific. The aqueous glutaraldehyde (cat #16210) was from EMS (Hatfield, PA, USA). All other reagents were of the purest grade from Sigma-Aldrich Co. (St. Louis, MO, USA).

2.2. Cell lines

The human osteosarcoma cell line MNNG/HOS (RRID: CVCL_0439) was obtained from the European Collection of Authenticated Cell Cultures (ECACC, Salisbury, UK) and grown at 37 °C, 5 % CO_2 in DMEM supplemented with 10 % FBS, 100 IU/ml penicillin, 100 μg/ml streptomycin, and 2 mM L-glutamine. Phenotypic characterization of these cells was monitored, as reported in our previous works [10,11].

2.3. Osteoblast primary cultures

Calvariae from 7-day-old mice were explanted, cleaned free of soft tissues and digested three times with 1 mg/ml *Clostridium histolyticum* type IV collagenase and 0.25 % trypsin, at 37 °C with gentle agitation for 15-, 30- and 45-min, according to well established protocols [12,13]. Cells from the second and third digestions were plated following centrifugation at 300*g* for 7 min and maintained in culture at 37 °C, 5 % CO_2 in DMEM plus 10 % FBS. At confluence, cells were trypsinized and plated according to the experimental protocol and are considered as neonatal mouse calvarial osteogenic cells.

2.4. Alkaline phosphatase activity assay

Neonatal mouse calvarial osteogenic cells were cultured for 2 days in standard conditions (serum free-DMEM, Control) or in presence of undiluted serum free-conditioned medium collected from osteogenic cells (OB-CM) or from MNNG/HOS cells (MNNG/HOS-CM) after 24 h of conditioning.

Parallel experiments were conducted culturing neonatal mouse calvarial osteogenic cells in mineralization medium (DMEM+10 % FBS supplemented with 10 mM β-glycerophosphate and 50 μg/ml ascorbic acid) and in mineralization medium supplemented with undiluted OB-CM or MNNG/HOS-CM for 7, 14 and 21 days of culture; during the timeframe of the experiment the culture medium was changed every 3 days. Osteogenic cells were then fixed in 4 % buffered paraformaldehyde for 10 min and washed twice with Dulbecco's Phosphate Buffered Saline (DPBS). Semi-quantitative histochemical detection of Alkaline phosphatase (Alp) activity (pH 9.3) was evaluated by a cytochemical assay employing the Sigma-Aldrich kit#86C-1KT, following the manufacturer's instruction.

2.5. Mineralization assay

Neonatal mouse calvarial osteogenic cells were cultured (5×10^4 cells in 6 multiwell plate, growth area: 9.6 cm^2) for 7, 14 and 21 days in 2 ml of mineralization medium (DMEM+10 % FBS supplemented with 10 mM β-glycerophosphate and 50 μg/ml ascorbic acid,) or in 2 ml of OB-CM or MNNG/HOS-CM (harvest from 2×10^4 cells cells in 6 multiwell plate, growth area: 9.6 cm^2 for 24 h) plus 10 mM β-glycerophosphate and 50 μg/ml ascorbic acid. During the timeframe of the experiment the culture medium was changed every 3 days, using fresh mineralizing DMEM, OB-CM or MNNG/HOS-CM; at the end, osteogenic cells were fixed in 4 % buffered paraformaldehyde for 10 min and washed twice with distilled water, then the presence of mineralization nodules was detected by von Kossa staining. Briefly, fixed osteogenic cells were incubated with 5 % aqueous solution of Silver Nitrate ($AgNO_3$) and exposed to ultraviolet light for 1 h; then cells were washed twice with distilled water, incubated with 5 % solution of Sodium Thiosulfate ($Na_2S_2O_3$) for 2 min, washed twice with distilled water, and air dried in a fume hood. Pictures of mineralization nodules (stained brown to black) were taken under an inverted phase-contrast microscope, and densitometric analysis was performed using NIH ImageJ tool.

2.6. 4′,6-Diamidino-2-phenylindole dihydrochloride staining

Neonatal mouse calvarial osteogenic cells were cultured for 7, 14 and 21 days in mineralization medium (DMEM+10 % FBS supplemented with 10 mM β-glycerophosphate and 50 μg/ml ascorbic acid) and in mineralization medium supplemented with undiluted OB-CM or MNNG/HOS-CM; during the timeframe of the experiment the culture medium was changed every 3 days. Neonatal mouse calvarial osteogenic cells were then fixed in 4 % buffered paraformaldehyde for 10 min, washed twice, and then stained with the nuclear dye 4′,6-Diamidino-2-phenylindole dihydrochloride (DAPI) (#D9542, Sigma-Aldrich) for 30 min in the dark at room temperature (RT), and analyzed by fluorescence microscopy.

2.7. Comparative real time PCR

RNA from neonatal mouse calvarial osteogenic cells cultured for 2 days in presence of undiluted conditioned medium collected from osteogenic cells (OB-CM) or from MNNG/HOS cells (MNNG/HOS-CM)

after 24 h of conditioning was extracted using TRIzol reagent, then 1 μg of RNA was reverse-transcribed into cDNA using the Moloney Murine Leukemia Virus (M-MLV) reverse transcriptase and subjected to real time PCR using primer pairs and amplification conditions described in Supplementary Table 1. All reactions were carried out using a SYBR green based master mix containing ROX as reference dye. Data were analyzed *via* dedicated software (MxPro, Stratagene, La Jolla, CA) using the ΔΔCt method and *Gapdh* was chosen as the housekeeping gene.

2.8. Nanoparticles isolation

Nanoparticles (NPs) from neonatal mouse calvarial osteogenic cells treated with OB-CM or MNNG/HOS-CM were isolated according to well established protocols [10,11,14]. Briefly, upon reaching 80 % confluence, neonatal mouse calvarial osteogenic cells were washed in DPBS and starved in serum free-DMEM to prevent contamination from FBS-NPs. Cells were maintained with serum-free DMEM or CM from OB-CM or MNNG/HOS-CM for 24 h. Following 3 times extensive washing to eliminate contaminating NPs, fresh DMEM was added [15,16]. For EVs harvesting, after 24 h the conditioned medium (CM) was collected and sequentially centrifuged at 300*g*, 4 °C for 5 min to remove dead cells and at 5000*g*, 4 °C for 25 min to remove membrane debris. The supernatant was collected and transferred to a Beckman L7-65 ultracentrifuge in a Beckman SW41-Ti or SW28 rotor and centrifuged at 100,000*g*, at 9 °C for 70 min. Supernatant was discarded, while the pellet, containing NPs, was resuspended in different buffers, according to the experimental needs. To quantify OB-NPs, they were subjected to nanoparticle tracking analysis as well as to protein extraction, the latter giving a mean yield of 4.5 ± 1.2 μg/12 ml CM. Freshly isolated NPs were used for all subsequent experiments.

2.9. Nanoparticles tracking analysis

Nanoparticles were isolated from CM (12 ml collected from one 182 cm^2 flask, cell density = 3.5×10^4 cells/cm^2) of neonatal mouse calvarial osteogenic cells treated for 24 h with OB-CM (CM_{OB}-OB-NPs) or MNNG/HOS-CM (CM_{HOS}-OB-NPs) and resuspended in 100 μl of filtered (0.22 μm) DPBS. NPs were then diluted 1:100 and used for nanoparticle tracking analysis using a nanosight NS300 NTA apparatus. Flow and camera gain were adjusted following the manufacturer's instructions based on the NS300 quality control parameters. Five camera acquisitions of 60 s each were analyzed for every biological replicate.

2.10. Western blot analysis

For cells and NPs protein extraction, samples were lysed in RIPA buffer (50 mM Tris HCl pH 7.5, 150 mM NaCl, 16.6 mM Nonidet P-40, 12.1 mM sodium deoxycholate, 3.47 mM SDS) containing protease inhibitors. Ten micrograms of NPs protein lysates, 50 μg of cell protein lysates and 40 μl of conditioned media were resolved by 10–15 % SDS-PAGE under reducing conditions and transferred to nitrocellulose membranes. Blots were incubated 2 h in 5 % nonfat dry milk in TBS-T, probed with the primary antibody in 1 % milk O/N at 4 °C or for 1 h at room temperature (RT), washed and incubated with the appropriate HorseRadish Peroxidase (HRP)-conjugated secondary antibody for 1 h at RT. After washing, protein bands were revealed using the SuperSignal Chemiluminescence substrate, according to the manufacturer's instructions, and acquired using a BioRad Gel Doc XR+ Imaging System. The analysis of band intensities was performed using the NIH ImageJ tool.

2.11. Transmission electron microscopy

Ten microliters of NPs isolated from CM (12 ml collected from one 182 cm^2 flask, cell density = 3.5×10^4 cells/cm^2) of osteogenic cells treated for 24 h with OB-CM (CM_{OB}-OB-NPs) or MNNG/HOS-CM (CM_{HOS}-OB-NPs) were fixed in 10 μl of 2 % glutaraldehyde for 30 min, put onto Formvar/Carbon coated grids and allowed to absorb for 20 min. Grids were then washed in distilled water, contrasted with 1 % phosphotungstic acid (PTA) for 2 min, washed again in distilled water and air-dried overnight. Samples were then observed under a Philips CM100 TEM (Transmission Electron Microscopy), with PHURONA camera (Emsis), at 80 kV.

2.12. Nanoparticles proteomics analysis and data processing

Shotgun proteomics were performed to evaluate the protein outfit of CM_{HOS}-OB-NPs compared to CM_{OB}-OB-NPs. NPs from three independent biological samples from each cell line were lysed by sonication on ice (Sonicator U200S control, IKA Labortechnik, Staufen, Germany) at 70 % amplitude in a lysis buffer (urea 6 M in 100 mM Tris/HCl, pH = 7.5). Bradford assay (Bio-Rad, Hercules, CA, USA) was used to taste the protein concentration by using Bovine Serum Albumin (BSA, Sigma-Aldrich, St. Louis, MI, USA) standard for the calibration curve in order to digest 20 μg of proteins for each NP sample obtaining two different pools (CM_{HOS}-OB-NPs and CM_{OB}-OB-NPs). Filter Aided Sample Preparation (FASP) protocol was used for overnight tryptic digestion at 37 °C. Each NPs sample was analyzed in triplicate by nanoLC-MS/MS through UltiMate™ 3000 UPLC (Thermo Fisher Scientific, Milan, Italy) chromatographic system coupled to the Orbitrap Fusion™ Tribrid™ (Thermo Fisher Scientific, Milan, Italy) mass spectrometer. All analytical parameters and specifications were detailed in Potenza et al. [17] setting the flow rate at 300 nL/min, with a total run time of 65 min using a chromatographic gradient from 2 % to 90 % of phase B (mobile phase A: 0.1 % formic acid in H_2O and mobile phase B: 0.1 % formic acid in acetonitrile). MaxQuant 1.6.10.50 and Perseus 1.6.10.50 (Max-Planck Institute for Biochemistry, Martinsried, Germany) were used for proteomics MS/MS raw data processing against the UniProt database (released 2020_06, taxonomy *Homo Sapiens*, 20,588 entries) and bioinformatics analysis, respectively. Processing parameters were set as reported in our previous works [17,18] in order to obtain LFQ Intensities, whose values were used to quantify protein abundance in each sample by comparing CM_{HOS}-OB-NPs *vs* CM_{OB}-OB-NPs (quantification in at least 2 out of 3 samples replicate, as reported also by Wei et al. [19]). SRplot tool (https://bioinformatics.com.cn/srplot) was used for graphical representation of proteomic data. Vesiclepedia tool (http://microvesicles.org) was used to confirm the vesicular nature of proteomic data. STRING tool (https://string-db.org) was used for Protein-Protein Interaction Networks Functional Enrichment Analysis. DAVID tool (https://david.ncifcrf.gov/tools.jsp) was used for Gene Ontology (GO) reclassification.

2.13. Statistics

Results are expressed as the mean ± SD of at least 3 independent experiments, as specified in the figure legends. Statistical analyses were performed using the paired Student's *t*-test, one sample *t*-test and ANOVA conducted either on raw data or on curves, according to the type of data. The statistical method used is indicated in each figure legend. A p value ≤ 0.05 was considered statistically significant. GraphPad Prism (version 9.0) was used to design graphs.

3. Results

3.1. Effect of osteosarcoma cells secretome on neonatal mouse calvarial osteoblast phenotype

To investigate whether osteosarcoma cells secretome could interfere with osteoblast phenotype, we treated neonatal mouse calvarial osteogenic cells (hereafter simply referred to as osteogenic cells) with serum free conditioned medium (CM) collected from MNNG/HOS (MNNG/HOS-CM) or with osteogenic cells-derived CM as control (OB-CM),

which also gives an indication of any autocrine effect. Osteogenic cells treated with serum free-DMEM were included as additional control. Although we are aware that 48 h serum-free conditions could reduce cell proliferation, we checked whether this culture condition could induce apoptosis, finding that it was not the case. In fact WB analysis for caspase-3 expression did not show the cleaved (*i.e.* active) form in any of our experimental conditions, while it was present in osteogenic cells treated with staurosporine (1 μM, 6 h) as positive control (Supp. Fig. 1a). Furthermore, these cells typically commit to the osteoblastic lineage upon exposure to mineralization medium, demonstrating a progressive increase in specific osteoblast markers throughout a 21-day culture period (Supp. Fig. 1b). Forty-eight hours of treatment with MNNG/HOS-

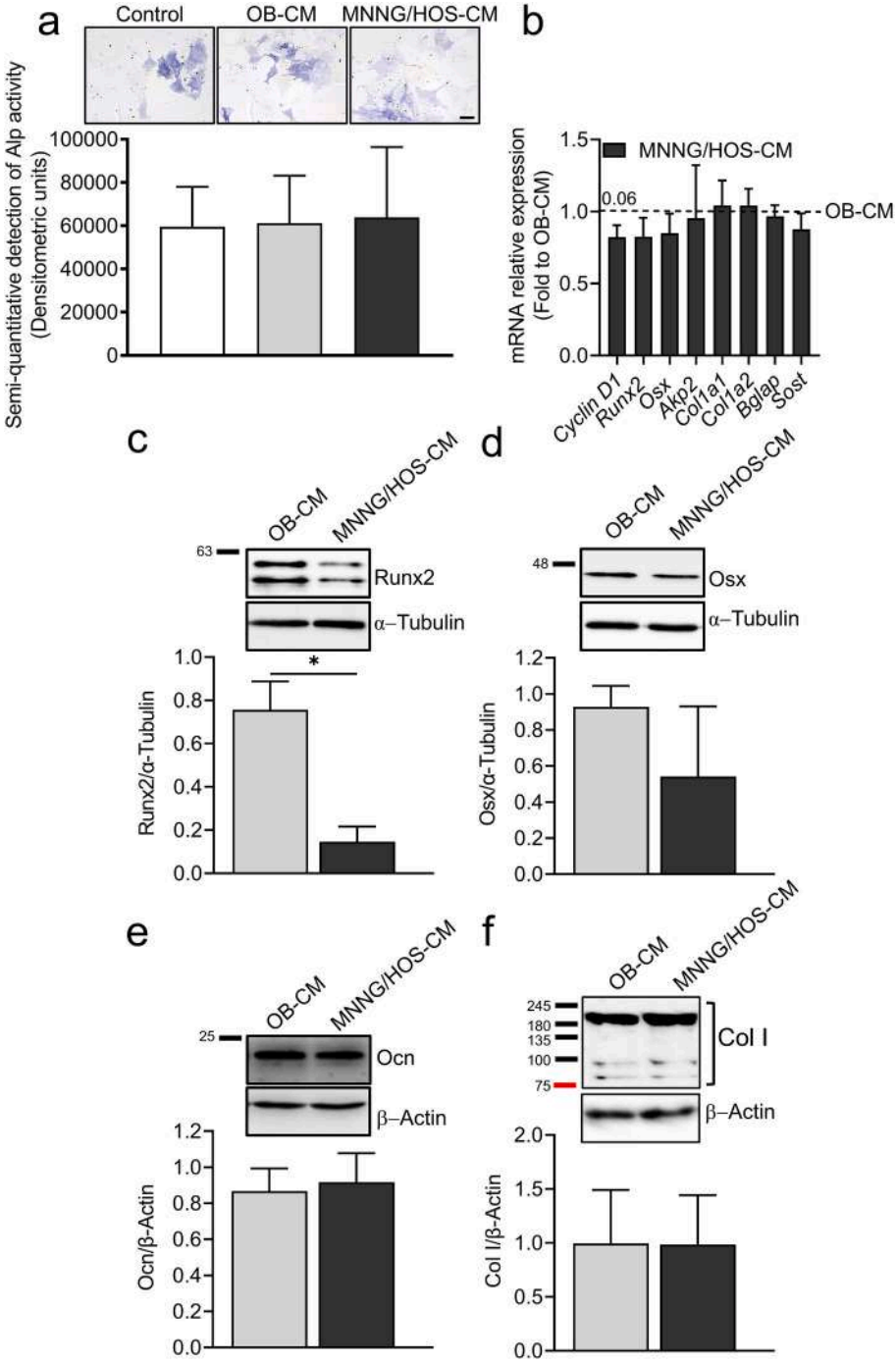

Fig. 1. Effect of MNNG/HOS secretome on neonatal mouse calvarial osteogenic cell phenotype: Neonatal mouse calvarial osteogenic cells were starved for 24 h, then medium was replaced with serum free-DMEM (Control) or with 24 h-serum free conditioned medium (CM) collected from neonatal mouse calvarial osteogenic cells (OB-CM) or from MNNG/HOS cells (MNNG/HOS-CM) and cells were cultured for further 48 h. (a) Representative pictures (inset) of cytochemical Alp activity and quantification by densitometric analysis (scale bar = 100 μm). (b) Real time RT-PCR analysis to evaluate the transcriptional expression of *Cyclin D1*, and of the osteoblastogenic genes *Runx2*, *Osterix* (*Osx*), *Akp2* (coding for Alkaline Phosphatase), *Collagen type I alpha 1 chain* (*Col1a1*) and *Col1a2*, *Bglap* (coding for Osteocalcin), and *Sclerostin* (*Sost*). (c–f) Western blot and densitometric analysis to evaluate protein expression of (c) Runt-related transcription factor 2 (Runx2), (d) osterix (osx), (e) osteocalcin (ocn) and Collagen I (Col I). Alfa-tubulin and β-actin were also evaluated as housekeeping genes, depending on the molecular weight of the target protein. Original uncropped WB with replicates is reported in Supplementary Figs. 1c–1f. Data are the mean ± SD of at least 3 independent experiments; $*p = 0.01$ *vs* OB-CM. (a, c–f)) paired *t*-test, (b) one-sample *t*-test.

derived secretome did not affect neither Alkaline Phosphatase (Alp) activity, one of the earliest markers of osteogenic cells differentiation (Fig. 1a) nor the transcriptional profile of osteogenic cells differentiating genes, while a trend of reduction ($p = 0.06$) was observed for Cyclin D1 mRNA (Fig. 1b). We next evaluated protein expression of the proosteogenic transcription factors Runt-related transcription factor 2 (Runx2) and Osterix (osx) finding that the former was significantly reduced by treatment with MNNG/HOS-CM (Fig. 1c, d), while the late osteogenic marker osteocalcin (ocn) was present at the same levels in both conditions (Fig. 1e). Also Collagen I protein expression (Col I) which is indicative of osteoblast function, was not affected by treatment (Fig. 1f).

Taken together, these results indicate that treatment for 48 h with MNNG/HOS secretome could affect osteoblast differentiation by a Runx2 dependent mechanism, while it did not alter the main functional markers; the lack of effect by osteoblast-CM treatment also excludes any autocrine conditioning.

We therefore decided to perform long-term treatments, refreshing the medium every 3 days. After 7 days of treatment, we observed no differences in Collagen I expression (Fig. 2a), although a likely immature form (Fig. 2a, bands at 180 kD) of Collagen showed a trend of decrease in osteogenic cells treated with MNNG/HOS-CM, as also demonstrated by densitometric analysis (Fig. 2a, graph). Interestingly, Collagen I release was dramatically reduced in osteogenic cells treated with MNNG/HOS compared to OB-CM treated or untreated osteogenic cells at 7, 14 and 21 days of culture in mineralization medium (Fig. 2b). No differences were found between untreated and OB-CM treated osteogenic cells.

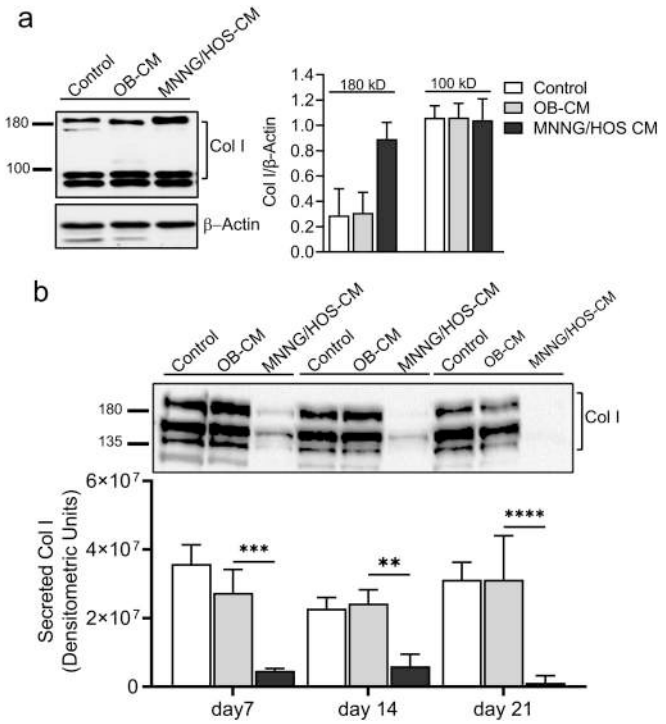

Fig. 2. Effect of MNNG/HOS secretome on neonatal mouse calvarial osteogenic cellactivity: (a) Neonatal mouse calvarial osteogenic cells were starved for 24 h, then medium was replaced with serum free-DMEM (Control) or with 24 h-serum free conditioned medium (CM) collected from neonatal mouse calvarial osteogenic cells (OB-CM) or from MNNG/HOS cells (MNNG/HOS-CM) and cells were maintained in cultures for 7 days, adding 10 % FBS after the first 48 h of treatment. Western blot analysis to evaluate collagen I protein expression and quantification of the higher (180 kD) and lower (100 kD) bands of Collagen I, the former likely an immature form, by densitometric analysis (graph). Beta-actin expression was also evaluated as housekeeping gene. (b) Western blot analysis for Collagen I release assessed in conditioned media (CM) collected from neonatal mouse calvarial osteogenic cells cultured in mineralization medium and treated with OB-CM and MNNG/HOS-CM at the times indicated in the abscissa. Original uncropped WB with replicates is reported in Supplementary Figs. 2a–2b. Data are the mean ± SD of at least 3independent experiments, $^{**}p < 0.01$, $^{***}p < 0.001$, $^{****}p < 0.0001$ *vs* OB-CM, two-way ANOVA.

We next asked whether this treatment may affect Alp activity, which was not the case at 7 days of treatment, while at day 14 and 21 a trend of reduction ($p = 0.1$) was observed in osteogenic cells treated with MNNG/HOS-CM compared to untreated or OB-CM treated osteogenic cells (Fig. 3a). Interestingly, osteoblast ability to produce nodules of mineralization, evaluated by von Kossa staining, was significantly impaired after 14 and 21 days of treatment with MNNG/HOS-CM (Fig. 3b). We also checked whether these modulations could be due to a direct effect on osteoblast number, finding that it was the case at 7 days of culture only, while at 14 days we observed a trend of reduction of osteoblast number by MNNG/HOS-CM, which however was unremarkable at 21 days of cultures (Fig. 3c).

Taken together, these results indicate that by means of their secretome and after prolonged treatment, osteosarcoma cells significantly reduce collagen production and bone matrix mineralization.

3.2. *Effect of osteosarcoma cells secretome on osteoblast release of nanoparticles*

Considering the pivotal role exerted by NPs in cell-cell communication, we investigated whether MNNG/HOS-CM could also interfere with the release and the protein cargo of osteoblast-derived NPs (OB-NPs). To this aim, we treated primary murine osteogenic cells with serum-free conditioned medium (CM) of MNNG/HOS cells or osteogenic cells, then we collected osteogenic cells NPs from the CM (CM_{HOS}-OB-NPs and CM_{OB}-OB-NPs, respectively). The vesicular nature of the isolated particles was confirmed by TEM, which also showed the NPs membrane integrity (Fig. 4a).

Nanosight analysis showed a similar mean diameter and number/ml of CM_{OB}-OB-NPs and CM_{HOS}-OB-NPs (Fig. 4b). Moreover, Western blot analysis demonstrated the expression of the typical NPs markers, such as Annexin II (Anxa II, Fig. 4c), CD63 (Fig. 4d), CD81 (Fig. 4e) and, interestingly, the latter was significantly upregulated in OB-NPs collected from osteogenic cells educated by MNNG/HOS-CM (CM_{HOS}-OB-NPs) compared to CM_{OB}-OB-NPs.

3.3. *Proteome profiling of osteoblast-derived nanoparticles preconditioned by osteosarcoma cells*

We next investigated whether MNNG/HOS secretome could educate OB-NPs protein cargo by performing shotgun proteomics analysis on NPs protein lysates, using a nano LC-MS/MS system. A total of 286 NP proteins were identified and quantified by this approach and, among them, 36 and 12 proteins were exclusively quantified in CM_{OB}-OB-NPs and CM_{HOS}-OB-NPs, respectively (Fig. 5a and Tables 1 and 2). Moreover, we found that 99 % (284 out of 286) of these proteins were present in the Vesiclepedia database, while 74 out of 286 (*i.e.* 26 %) were included in the top 100 NP-Proteins reported in the database, suggesting a good enrichment. Using STRING platform, we investigated the Protein-Protein Interaction (PPI) network of the 36 proteins exclusively present in CM_{OB}-OB-NPs, finding an enrichment of proteins involved in cell junction network, such as Protein deglycase DJ-1 (Park/DJ-1), 60S ribosomal protein L18 (RpL18), 40S ribosomal protein S18 (RpS18), RpL30, Proteasome subunit alpha type-7 (Psma7), Carboxypeptidase E (CpE), WD repeat-containing (Wdr1), Radixin (Rdx), Ptk7, Uba1, Pppr1a, Adam10, Rab18, Rab7, vesicle-associated membrane protein 3 (Vamp3) and Syntaxin-4 (Stx4) was observed (Fig. 5b; blue nodes; FDR $= 3.91 \times 10^{-5}$), while no significant networks have been identified for the 12 proteins exclusively present in CM_{HOS}-OB-NPs (Fig. 5c).

We next focused on the 238 common expressed proteins and ran univariate statistical analysis through Perseus tool using a cut-off value

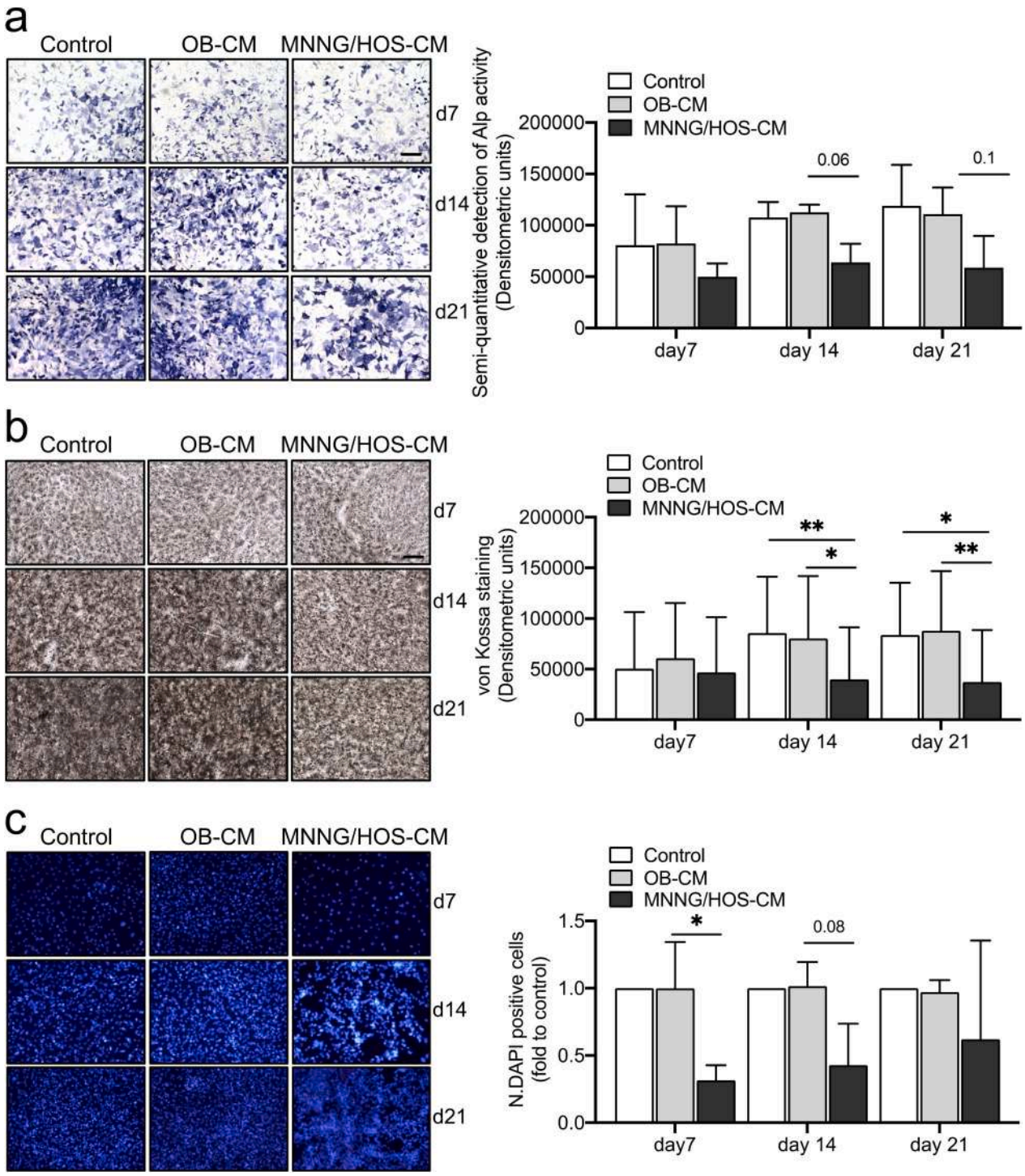

Fig. 3. Effect of MNNG/HOS secretome on neonatal mouse calvarial osteogenic cell activity: Neonatal mouse calvarial osteogenic cells were cultured in mineralization medium (Control) and in mineralization medium supplemented with OB-CM or MNNG/HOS-CM for 7, 14 and 21 days. (a) Representative pictures (inset) of osteogenic cells subjected to cytochemical Alp activity and quantification by densitometric analysis (scale bar = 500 μm). (b) Representative pictures (inset) of Von Kossa staining to evaluate nodules of mineralization and quantification by densitometric analysis (scale bar = 500 μm). (c) Representative pictures (inset) of osteogenic cells subjected to DAPI staining and quantification of the number of positive nuclei/field (scale bar = 500 μm). Data are the mean ± SD of 3 independent experiments, *$p < 0.05$ *vs* OB-CM, **$p < 0.01$ *vs* CTRL; (a, b) paired Student's *t*-test, (c) one-sample *t*-test.

of $p < 0.05$, which revealed the presence of 58 differentially expressed proteins (DEPs), among which 26 proteins were downregulated (Table 3) and 32 proteins were upregulated (Table 4) in CM_{HOS}-OB-NPs compared to CM_{OB}-OB-NPs (Fig. 5d).

Hence, to deeply characterize the pathways and processes in which these DEPs could be involved, we performed gene ontology (GO) analysis using DAVID tool and a cut-off value of FDR < 0.05. GO of biological processes revealed that most of the proteins were significantly enriched in elastic fiber assembly, microtubule-based processes, and collagen fibril organization (Fig. 6a). Moreover, GO analysis of cellular components identified proteins significantly enriched in collagen type I trimer, collagen type XI trimer, and basement membrane components

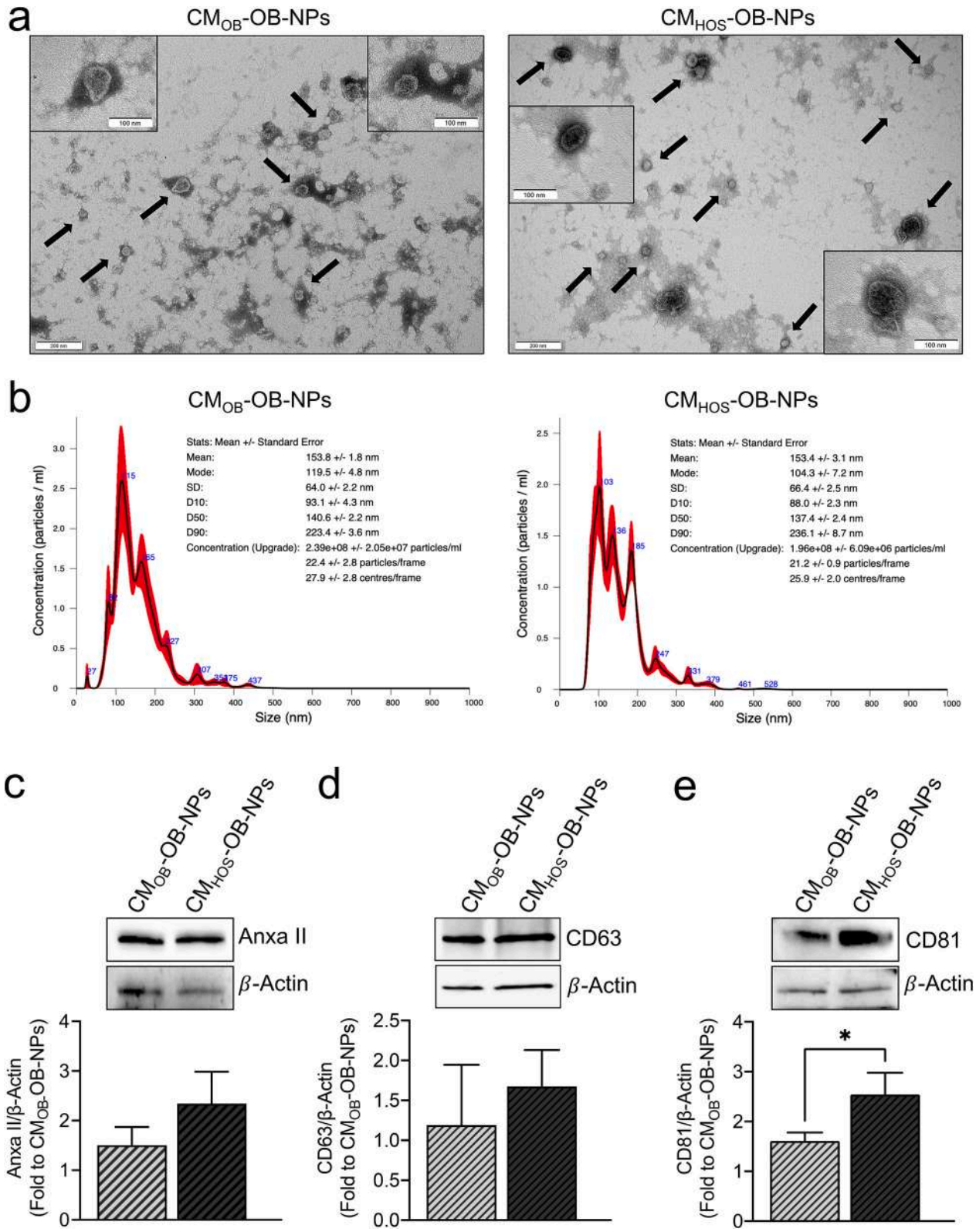

Fig. 4. Characterization of nanoparticles (NPs) isolated from neonatal mouse calvarial osteogenic cells treated with OB-CM or MNNG/HOS-CM: Neonatal mouse calvarial osteogenic cells were starved for 24 h, then medium was replaced with serum free conditioned medium (CM) collected from neonatal mouse calvarial osteogenic cells (OB-CM) or from MNNG/HOS cells (MNNG/HOS-CM). After 24 h, neonatal mouse calvarial osteogenic cells were washed and maintained for further 24 h in serum-DMEM, then conditioned media were collected to isolate NPs. (a) Transmission electron microscopy (TEM) evaluation of the morphology of NPs (indicated by arrows) isolated from neonatal mouse calvarial osteogenic cells educated with OB-NPs) or with MNNG/HOS-CM (CM_{HOS}-OB-NPs). Scale bar = 200 μm. Insets: higher magnification of the same NPs sample (scale bar = 100 μm). (b) Size and concentration determination of CM_{OB}-OB-NPs and CM_{HOS}-OB-NPs by nanoparticle tracking analysis (NanoSight NS3000). (c–e) Western blot and densitometric analysis to evaluate protein expression of the NP markers (c) Annexin II (Anxa II), (d) CD63 and (e) CD81, and β-Actin as loading control in protein lysates (10 μg) extracted from CM_{OB}-OB-NPs and CM_{HOS}-OB-NPs. Original uncropped WB with replicates is reported in Supplementary Figs. 4c–4f. Data are the mean ± SD of three independent preparations, $*p = 0.025$ *vs* paired Student's *t*-test.

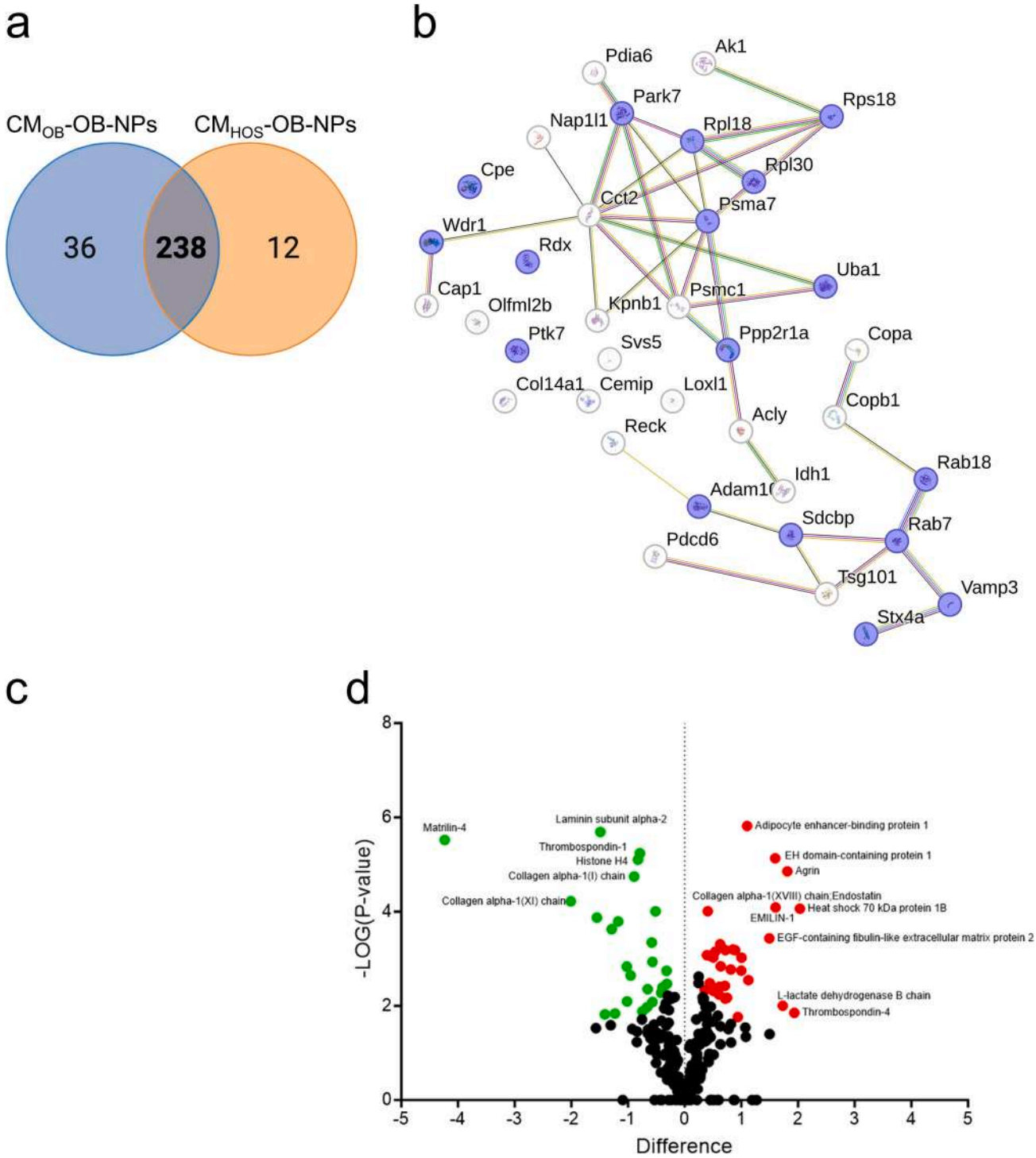

Fig. 5. Proteome profiling of nanoparticles (NPs) isolated from osteogenic cells treated with OB-CM or MNNG/HOS-CM: Neonatal mouse calvarial osteogenic cells were starved for 24 h, then medium was replaced with serum free-DMEM (Control) or with 24 h-conditioned medium (CM) collected from neonatal mouse calvarial osteogenic cells (OB-CM) or from MNNG/HOS cells (MNNG/HOS-CM). After 24 h, osteogenic cells were washed and maintained for further 24 h, then conditioned media were collected to isolate NPs and perform proteome analysis. (a) Representative Venn diagram showing the number of unique and commonly shared proteins between CM_{OB}-OB-NPs and CM_{HOS}-OB-NPs groups. (b) Representative Protein-Protein Interaction (PPI) network of proteins uniquely quantified in CM_{OB}-OB-NPs, generated by STRING online tool. Nodes represent proteins ($N = 36$), and edges indicate the number of interactions ($N = 38$). Color saturation of the edges represents the confidence score of a functional association. The number of average interactions per node is indicated by the node degree ($N = 2.11$). The clustering coefficient specifies the average node density of the map ($N = 0.427$). Only interactions with a medium confidence score ≥ 0.4 are shown. (c) Representative PPI network of proteins only quantified in CM_{HOS}-OB-NPs, generated by STRING online tool. Nodes represent proteins ($N = 12$), and edges indicate the number of interactions ($N = 7$). Color saturation of the edges represents the confidence score of a functional association. The number of average interactions per node is indicated by the node degree ($N = 1.17$). The clustering coefficient specifies the average node density of the map ($N = 0.375$). Only interactions with a medium confidence score ≥ 0.4 are shown. (d) Volcano plot representation of differential expressed proteins (DEPs) among CM_{OB}-OB-NPs and CM_{HOS}-OB-NPs groups. Red and green dots highlight significantly upregulated or downregulated proteins in CM_{HOS}-OB-NPs *versus* CM_{OB}-OB-NPs, respectively (P-value < 0.05). The x-axis shows the difference in proteins expression and the y-axis $-$LOG(P-Value) rate of proteins being differentially expressed.

Table 1
List of the proteins exclusively expressed by NPs isolated from osteogenic cells educated with OB-CM.

Protein name	Gene name	Intensity sample #1	Intensity sample #2	Intensity sample #3	Mean intensity
Syntenin-1	*Sdcbp*	28,922,000	17,143,000	18,599,000	21,554,667
Adenylyl cyclase-associated protein 1	*Cap1*	7,061,700	6,065,200	6,190,000	6,438,967
Semenogelin-1	*Semg1*	7,759,400	5,472,500	5,504,900	6,245,600
Lysyl oxidase homolog 1	*Loxl1*	5,220,200	4,545,800	5,583,700	5,116,567
T-complex protein 1 subunit beta	*Cct2*	4,841,900	5,793,700	4,579,500	5,071,700
Proteasome subunit alpha type-7	*Psma7*	4,042,900	3,937,900	5,004,100	4,328,300
Ras-related protein Rab-7a	*Rab7A*	2,906,100	2,920,600	2,884,200	2,903,633
Inactive tyrosine-protein kinase 7	*Ptk7*	2,599,100		2,698,200	2,648,650
Olfactomedin-like protein 2B	*Olfml2B*	3,009,000	2,217,800	2,480,900	2,569,233
Protein deglycase DJ-1	*Park7*	2,583,800	2,425,300	1,975,500	2,328,200
40S ribosomal protein S18	*RpS18*	2,246,800	2,402,500	2,123,300	2,257,533
Ubiquitin-like modifier-activating enzyme 1	*Uba1*	2,261,400	2,145,900	2,267,700	2,225,000
ATP-citrate synthase	*Acly*	2,003,400	2,345,400	2,305,600	2,218,133
Syntaxin-4	*Stx4*	2,268,500	2,284,600	2,082,700	2,211,934
Vesicle-associated membrane protein 3	*Vamp3*	1,521,400	1,911,800	2,524,500	1,985,900
Adenylate kinase isoenzyme 1	*Ak1*	1,603,000	1,559,500	1,738,800	1,633,767
Importin subunit beta-1	*KpnB1*	1,265,600	1,839,900	1,447,900	1,517,800
WD repeat-containing protein 1	*Wdr1*	1,184,500	1,784,100	1,548,200	1,505,600
Serine/threonine-protein phosphatase 2A 65 kDa regulatory subunit A alpha isoform	*Pppr1A*	1,096,400	1,665,500	1,713,600	1,491,833
60S ribosomal protein L18	*RpL18*	1,692,700	1,326,900	1,388,800	1,469,467
Nucleosome assembly protein 1-like 1	*Nap1l1*	1,205,800	1,711,500	1,444,700	1,454,000
60S ribosomal protein L30	*RpL30*	1,001,600	1,512,600	1,707,200	1,407,133
Ras-related protein Rab-18	*Rab18*		1,211,100	1,540,500	1,375,800
Collagen alpha-1(XIV) chain	*Col14A1*	1,452,500	1,259,400	1,351,800	1,354,567
Cell migration-inducing and hyaluronan-binding protein	*Cemip*	917,060	1,811,900	1,039,600	1,256,187
26S protease regulatory subunit 4	*Psmc1*	1,363,900		914,240	1,139,070
Programmed cell death protein 6	*Pdcd6*	873,120		1,318,700	1,095,910
Carboxypeptidase E	*Cpe*	996,570	1,124,000		1,060,285
Disintegrin and metalloproteinase domain-containing protein 10	*Adam10*		967,480	1,013,700	990,590
Coatomer subunit alpha	*CopA*	798,280	1,145,100	990,780	978,053
Protein disulfide-isomerase A6	*PdiA6*	659,190	899,590	924,310	827,697
Isocitrate dehydrogenase [NADP] cytoplasmic	*Idh1*		966,210	670,640	818,425
Radixin	*Rdx*		552,560	814,381	683,470
Reversion-inducing cysteine-rich protein with Kazal motifs	*Reck*	683,490	611,110	677,050	657,217
Tumor susceptibility gene 101 protein	*Tsg101*	570,180	635,600		602,890
Coatomer subunit beta	*CopB1*		507,350	687,550	597,450

Table 2
List of the proteins exclusively expressed by NPs isolated from osteogenic cells educated with MNNG/HOS-CM.

Protein name	Gene name	Intensity sample #1	Intensity sample #2	Intensity sample #3	Mean intensity
Insulin-like growth factor-binding protein 5	*Igfbp5*	5,505,900	5,388,900		5,447,400
Fibronectin type III domain-containing protein 1	*Fndc1*	6,111,400	4,069,000	4,703,000	4,961,133
Amyloid beta A4 protein	*App*	5,787,600	3,728,200	4,053,100	4,522,967
T-complex protein 1 subunit eta	*Cct7*	3,900,400	4,451,800	3,844,000	4,065,400
Septin-2	*Sept2*	2,710,900		3,569,100	3,140,000
Podocan	*Podn*	3,345,000	2,961,900	2,795,000	3,033,967
Protein disulfide-isomerase A3	*Pdia3*	2,485,100		2,602,700	2,543,900
40S ribosomal protein S11	*RpS11*	2,472,100	2,406,100		2,439,100
Keratinocyte proline-rich protein	*Kprp*		2,751,100	2,112,700	2,431,900
Stress-70 protein, mitochondrial	*Hspa9*	1,804,900	2,051,300	2,846,100	2,234,100
Band 4.1-like protein 3	*Epb41l3*		1,434,600	2,302,600	1,868,600
26S proteasome non-ATPase regulatory subunit 3	*Psmd3*	1,464,800	1,384,700	1,619,900	1,489,800

(Fig. 6b), while GO enriched molecular functions included, among all, extracellular matrix structural constituents conferring tensile strength, proteoglycan binding, and collagen binding (Fig. 6c). Finally, Kyoto Encyclopaedia of Genes and Genomes (KEGG) pathway analysis revealed that proteins were significantly enriched in ECM-receptor interaction, and in protein digestion and absorption (Fig. 6d).

Taken together, these findings suggest that MNNG/HOS secretome exerts a direct effect on osteoblast-NPs, reprogramming their protein profile and subsequently influencing extracellular matrix composition and collagen formation, as corroborated by *in vitro* data.

Since GO and KEGG analyses on the 58 DEPs gave us a global view of the processes and pathways influenced by MNNG/HOS cells secretome, we used STRING platform to perform a functional enrichment analysis of the Protein-Protein Interaction network (PPI). As described in Fig. 7a, among the downregulated NP proteins identified in OB-NPs from MNNG/HOS-educated osteogenic cells, we found: i) proteins involved in the extracellular matrix organization, such as matrillin (Matn)4 and Matn2, and collagens, such as Col Iα_1, Col Iα_2, Col IIα_1, Col Vα_1, Col XIα_1 (green nodes; FDR $= 5.04 \times 10^{-5}$), ii) extracellular matrix structural constituents (red nodes; FDR $= 1.71 \times 10^{-7}$), such as Laminin (Lama) 2 and collagens, and iii) collagen-containing extracellular matrix (Anxa4, Matn2, Matn4, Gpc1, Thbs1, Nid2, Lama2, Col Iα_1, Col Iα_2, Col IIα_1, Col Vα_1, Col VIα_1, Col VIα_2, Col XIα_1, blue nodes; FDR $= 1.17 \times 10^{-16}$). We then focused on the most downregulated protein, that is Matn4 (Fold Change $= -4.23$, $p = 3.32 \times 10^{-6}$), due to its role as a downstream orchestrator of the collagens network and confirmed, by Western blot, that pretreatment with MNNG/HOS-CM significantly reduced its content in the OB-NPs (Fig. 7b).

Table 3
List of the downregulated proteins expressed by NPs from osteogenic cells educated with MNNG/HOS-CM compared to OB-CM.

Protein names	Gene names	Intensity	−LOG(P-value)	Difference
Matrilin-4	*Matn4*	176,420,000	5.52070607	−4.2329661
Collagen alpha-1(XI) chain	*Col11a1*	39,247,000	4.21926429	−2.0078259
Collagen alpha-1(II) chain;Collagen alpha-1(II) chain;Chondrocalcin	*Col2a1*	427,360,000	3.87160898	−1.5489642
Laminin subunit alpha-2	*Lama2*	55,176,000	5.69126321	−1.4864807
Pappalysin-2	*Pappa2*	10,666,000	1.8199685	−1.4071903
EGF-like repeat and discoidin I-like domain-containing protein 3	*Edil3*	415,360,000	3.62636911	−1.286684
Collagen alpha-1(V) chain	*Col5a1*	93,524,000	1.83667725	−1.2272917
Clathrin heavy chain 1	*Cltc*	143,950,000	3.79122046	−1.1728713
Glypican-1;Secreted glypican-1	*Gpc1*	9,405,000	2.83164664	−1.0200551
Proteasome subunit alpha type-3	*Psma3*	25,011,000	2.09326969	−1.0150553
Histone H2B type 1-L;Histone H2B type 1-M;Histone H2B type 1-N;Histone H2B type 1-H;Histone H2B type 2-F;Histone H2B type 1-C/E/F/G/I;Histone H2B type 1-D;Histone H2B type F-S;Histone H2B type 1-K;Histone H2B type 1-A	*Hist1h2bl;Hist1h2bm;Hist1h2bn;Hist1h2bh; Hist2h2bf;Hist1h2bc;Hist1h2bd;H2bfs; Hist1h2bk;Hist1h2ba*	717,220,000	2.6438692	−0.9525706
Collagen alpha-1(I) chain	*Col1a1*	2.1285E+10	4.74550161	−0.890274
Histone H4	*Hist1h4a*	879,440,000	5.10249649	−0.8248564
Thrombospondin-1	*Thbs1*	364,600,000	5.23887335	−0.7891598
Annexin A4	*Anxa4*	51,814,000	1.88090213	−0.7453238
Histone H3.2;Histone H3.1t;Histone H3.3;Histone H3.1;Histone H3.3C	*Hist2h3a;Hist3h3;H3f3a;Hist1h3a;H3f3c*	230,280,000	1.96855332	−0.6635145
Matrilin-2	*Matn2*	17,788,000	2.35433429	−0.6535676
Collagen alpha-1(VI) chain	*Col6a1*	205,760,000	3.34345265	−0.5789572
Collagen alpha-2(VI) chain	*Col6a2*	78,024,000	2.93384691	−0.5674807
Histone H2A type 1-J;Histone H2A type 1-H;Histone H2A.J;Histone H2A type 2-C;Histone H2A type 2-A;Histone H2A type 1-D;Histone H2A type 1	*Hist1h2aj;Hist1h2ah;H2afj;Hist2h2ac; Hist2h2aa3;Hist1h2ad;Hist1h2ag*	432,340,000	2.08188306	−0.5673428
Nidogen-2	*Nid2*	224,190,000	4.0055587	−0.5129045
Annexin A2;Putative annexin A2-like protein	*Anxa2;Anxa2p2*	645,260,000	2.2776614	−0.4123128
Collagen alpha-2(I) chain	*Col1a2*	3,187,900,000	2.27678111	−0.4041341
Dickkopf-related protein 3	*Dkk3*	10,543,000	2.38900264	−0.389356
Tubulin alpha-1B chain;Tubulin alpha-1C chain;Tubulin alpha-1A chain;Tubulin alpha-4A chain;Tubulin alpha-8 chain;Tubulin alpha-3E chain	*Tuba1b;Tuba1c;Tuba1a;Tuba4a;Tuba8; Tuba3e*	158,480,000	2.74436085	−0.3184191
Vimentin	*Vim*	670,390,000	2.46657485	−0.3152637

Similarly, among the NP proteins isolated from MNNG/HOS-educated osteogenic cells, the PPI analysis showed an increased content of: i) proteins involved in the regulation of collagen fibril organization (Fig. 7c; green nodes; FDR = 0.0016), such as EGF-containing fibulin-like extracellular matrix protein 2 (Efemp2), Adipocyte enhancer-binding protein-1 (Aebp1) and Emilin1, ii) extracellular matrix structural constituents (Fig. 7c; red nodes; FDR = 0.00023), such as Emilin-1 and collagens (Col IIIα_1, Col IVα_2, Col Vα_2, Col XVIIIα_1), and iii) collagen-containing extracellular matrix (Fig. 7c; blue nodes; FDR = 2.44×10^{-11}), such as Pyruvate kinase PKM (Pkm), SPARC-related modular calcium-binding protein 1 (Smoc1), Angiopoietin-related protein 2 (Angptl2), Hsp90α, Agrin (Agrn), Bmp1, thrombospondin 4 (Thbs4), Efemp2 and collagens (Col IIIα_1, Col IVα_2, Col Vα_2, Col XVIIIα_1).

4. Discussion and conclusion

Osteosarcoma is a high-grade tumor of bone deriving from a malignant transformation of MSCs, leading to the production of an osteoid-like matrix with different degrees of mineralization [5]. Osteosarcoma growth strictly relies on a complex crosstalk among tumor cells, resident cells, and the bone matrix [5,6]. With this in mind, we treated osteogenic cells with MNNG/HOS derived secretome for a short period of time (*i.e.* 2 days), which, apart from a reduction of the master gene Runx2, failed to influence the transcriptional and protein expression of genes related to osteoblast differentiation and activity. The specific downregulation of Runx2 without observable effects on osteoblast activity markers, at the time points examined, suggests that the tumoral secretome inhibits osteogenic differentiation at its earliest stages by targeting the upstream master regulator Runx2, requiring downstream differentiation markers additional days to reflect this inhibition, consistent with protein turnover rates. Alternatively, the tumor secretome might selectively uncouple osteogenic differentiation from osteoblast function. However, this observation aligns with previously reported mechanisms in tumor cell-osteoblast crosstalk, making it a plausible biological event [20,21]. Since it is known that tumor cells are able to deregulate the extracellular matrix components, we wonder whether osteosarcoma-derived secretome could educate osteogenic cells production and release of the main constituent of the bone matrix, that is Collagen type I, as well as osteocalcin, which is also a late marker of osteoblast differentiation, however this was not the case. Nevertheless, we asked whether a prolonged exposure to MNNG/HOS secretome could influence osteoblast phenotype, finding a trend of reduction of ALP activity, one of the early markers of osteoblast differentiation, after 14 and 21 days of treatment, along with a reduction, at least after 7 and 14 days of culture of osteoblast number. This effect is observed in osteogenic cells cultured in the presence of a mineralization medium, which also has osteogenic properties. Interestingly, education of osteogenic cells with MNNG/HOS secretome significantly reduced Collagen type I release and deposition already at 7 days of treatment, and this reduction is more consistent after 21 days of treatment. Again, no differences are observed between untreated osteogenic cells and osteogenic cells treated with osteoblast-derived secretome. Consistent with a lesser content of Collagen type I, MNNG/HOS secretome-educated osteogenic cells showed a lower ability to form nodule of mineralization. This interesting result is in line with Cmoch et al., who found that stimulation of mineralization by treating osteosarcoma cells with ascorbic acid and B-glycerophosphate impaired their invasive properties by inhibiting invadopodia formation [22].

Taken together, this data demonstrates that osteosarcoma-derived secretome primarily affects neonatal mouse calvarial osteoblast's function and number, eventually leading to a bone matrix whose composition in terms of quantity of collagen fibres and nodule of mineralization is impaired, thus concurring to the production of a pathogenic osteoid matrix.

It is well known the crucial role exerted by NPs in the crosstalk between osteogenic cells and tumor cells. Therefore, we next investigated whether osteosarcoma cells secretome is able to influence the release of osteoblast-NPs as well as NPs protein profile. We found no significant difference in terms of NPs content and size released by neonatal mouse

Table 4
List of the upregulated proteins expressed by NPs from osteogenic cells educated with MNNG/HOS-CM compared to OB-CM.

Protein names	Gene names	Intensity	−LOG(P-value)	Difference
Heat shock 70 kDa protein 1B;Heat shock 70 kDa protein 1A	*Hspa1b*; *Hspa1a*	54,339,000	4.06088885	2.03280258
Thrombospondin-4	*Thbs4*	132,570,000	1.85001867	1.93524551
Agrin;Agrin N-terminal 110 kDa subunit;Agrin C-terminal 110 kDa subunit;Agrin C-terminal 90 kDa fragment;Agrin C-terminal 22 kDa fragment	*Agrn*	73,875,000	4.85331711	1.81249746
L-lactate dehydrogenase B chain	*Ldhb*	66,257,000	2.00185451	1.73106257
Emilin-1	*Emilin1*	145,570,000	4.08815299	1.60500654
EH domain-containing protein 1	*Ehd1*	42,768,000	5.13206462	1.59648577
EGF-containing fibulin-like extracellular matrix protein 2	*Efemp2*	170,720,000	3.43182328	1.49389267
Angiopoietin-related protein 2; Angiopoietin-like protein 2	*Angptl2*	6,454,600	2.54736274	1.12344233
Adipocyte enhancer-binding protein 1	*Aebp1*	196,600,000	5.81770225	1.10289383
Cytoplasmic FMR1-interacting protein 1	*Cyfip1*	9,914,700	3.02297916	1.00271924
Heat shock protein HSP 90-alpha	*Hsp90aa1*	26,915,000	2.74798171	0.99891027
MARCKS-related protein	*Marcksl1*	9,977,700	1.76310088	0.93705591
Collagen alpha-1 (III) chain	*Col3a1*	1,442,200,000	3.18121429	0.89073181
Follistatin-related protein 1	*Fstl1*	169,500,000	3.19555273	0.85017331
Ras-related protein Rap-1b;Ras-related protein Rap-1b-like protein	*Rap1b*	67,189,000	2.76982559	0.81293933
SPARC-related modular calcium-binding protein 1	*Smoc1*	18,267,000	2.17013636	0.7474378
EH domain-containing protein 4	*Ehd4*	21,564,000	3.18070672	0.71789932
ADP-ribosylation factor 1;ADP-ribosylation factor 3	*Arf1;Arf3*	14,561,000	2.15182204	0.71670151
Peroxiredoxin-6	*Prdx6*	6,392,000	2.42390695	0.7093722
Myosin-9	*Myh9*	119,610,000	2.83773712	0.63712756
Triosephosphate isomerase	*Tpi1*	61,900,000	3.30872312	0.62577184
14-3-3 protein gamma;14-3-3 protein gamma, N-terminally processed	*Ywhag*	88,577,000	2.4032687	0.61179479
T-complex protein 1 subunit theta	*Cct8*	31,896,000	2.23734932	0.60697492
Bone morphogenetic protein 1	*Bmp1*	29,794,000	3.15288937	0.53964996
14-3-3 protein epsilon	*Ywhae*	56,843,000	2.31091587	0.51879374
Collagen alpha-2 (IV) chain; Canstatin	*Col4a2*	41,082,000	3.02652277	0.50358772
Fructose-bisphosphate aldolase A	*Aldoa*	113,270,000	2.33841695	0.4782842
Peroxiredoxin-1	*Prdx1*	47,022,000	3.05399173	0.46403821
GTP-binding nuclear protein Ran	*Ran*	23,875,000	2.48040243	0.44186783
Collagen alpha-1 (XVIII) chain; Endostatin	*Col18a1*	26,430,000	4.00811379	0.40743128
Pyruvate kinase PKM	*Pkm*	115,230,000	3.07514333	0.39375242
Collagen alpha-2(V) chain	*Col5a2*	472,230,000	2.33175076	0.3542188

calvarial osteogenic cells subjected to an autocrine regulation *versus* osteogenic cells educated by MNNG/HOS-CM, however in the latter we observed a higher expression of the NPs marker CD81. Besides the role of this tetraspanin as a NPs marker, it is noteworthy that CD81 has also been described as a protumoral factor in osteosarcoma. Indeed, Li et al. found CD81 to be one of the genes aberrantly regulated in human osteoblast FOB1.19 cells transformed by treatment with the carcinogenic promoting agent 12-O-tetradecanoyl phorbol-13-acetate (TPA) [23]. Consistently, Mizishori et al. [24] found that inhibition of CD81 reduces tumorigenesis and lung metastasis in osteosarcoma cells.

Regarding proteomic analysis, we identified 238 proteins commonly present in both types of OB-NPs, while 36 and 12 proteins were uniquely detected in CM_{OB}-OB-NPs and CM_{HOS}-OB-NPs, respectively. While current technological limitations make it challenging to effectively distinguish between proteins intrinsically constituting NPs and those present in the microenvironment and subsequently docked to their surface, which form the so-called "corona coating", the biological meaning of these proteins remains undiminished, playing a crucial role in the biological context of NPs functions. Looking at the shared proteins, and in agreement with the *in vitro* data, we found that treatment with osteosarcoma secretome downregulates Col Iα_1 and Col Iα_2 expression in NPs, along with other collagens (Col XIα_1, Col IIα_1, Col Vα_1, Col VIα_1 and α_2) as well as bone matrix proteins like Laminin α2 subunits, Nidogen-2, Thrombospondin-1 and the proteoglycan Glypican-1. However, also among the upregulated proteins we found some collagens, such as Col IIIα_1, Col IVα_2, Col XVIIIα_1, and Col Vα_2, as well as Thrombospondin-4. Therefore, osteosarcoma secretome downregulates the expression of Collagen type I, which is the most abundant component (>90 %) of the organic part of the bone matrix and deregulates the expression of other collagens and non-collagen proteins of the bone matrix, eventually leading to an aberrant expression of the bone matrix constituents. Of note, and consistent with the above results, the most downregulated protein resulted to be Matn4 [24,25], and downregulation of Matn2 was also observed. These proteins are members of the matrilin family, which includes four oligomeric extracellular proteins that are involved in the development and homeostasis of cartilage and bone [26]. While Matn1 (also known as cartilage matrix protein or CMP) and Matn3 are mainly expressed in cartilage and have a role in cartilage and bone development, Matn2 and 4 are present in a wide variety of extracellular matrices [27], where they exert a prominent role in stabilizing the extracellular matrix structure, by self-associating into supramolecular structures, resulting in the formation of filamentous networks [27]. Therefore, by downregulating these proteins, MNNG/HOS secretome likely impairs the bone matrix structure.

Going to analyze the upregulated proteins found in OB-NPs isolated

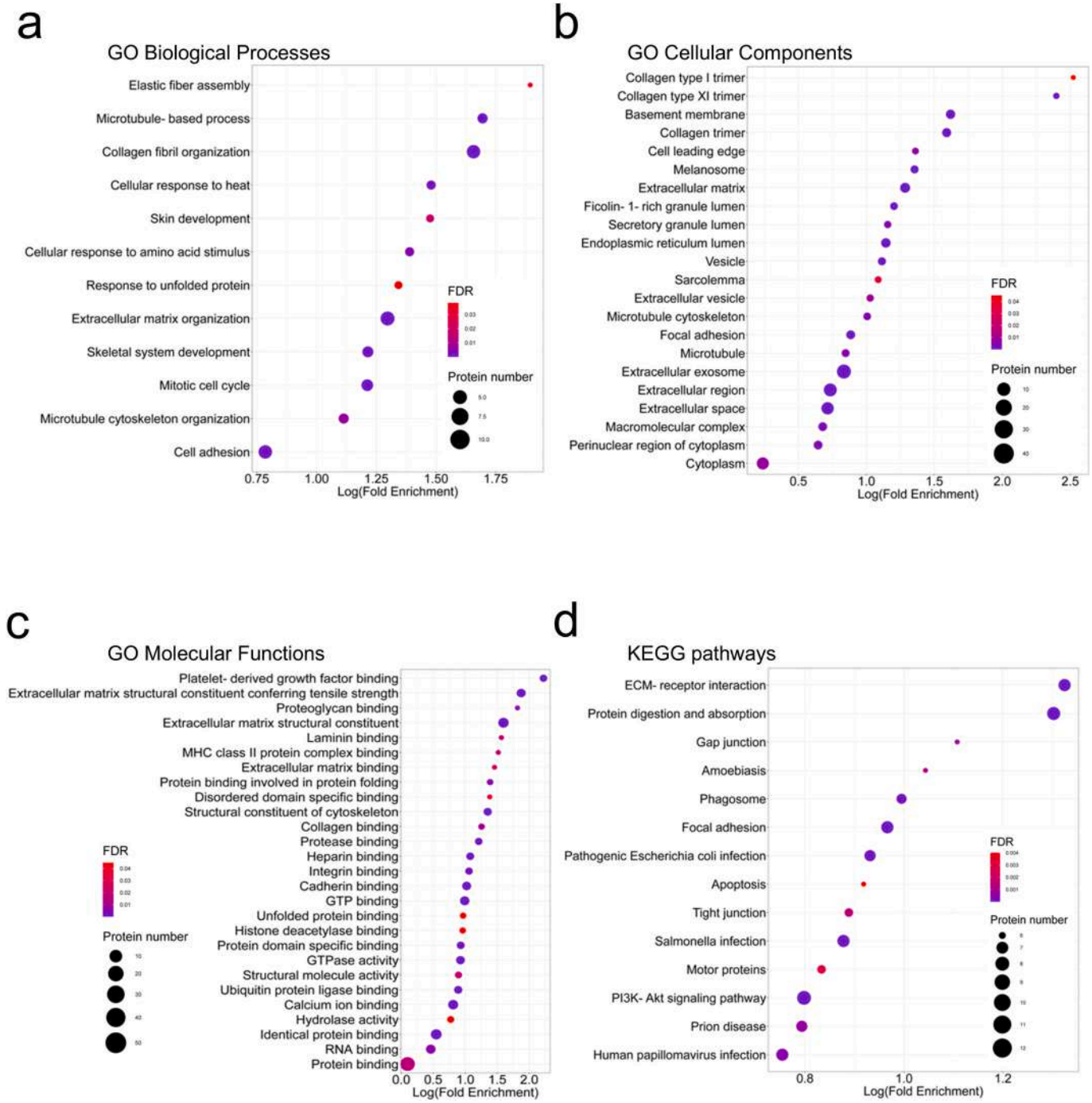

Fig. 6. Gene ontology (GO) enrichment analysis of DEPs between CM_{OB}-OB-NPs and CM_{HOS}-OB-NPs Neonatal mouse calvarial osteogenic cells were starved for 24 h, then medium was replaced with serum free-DMEM (Control) or with 24 h-conditioned medium (CM) collected from neonatal mouse calvarial osteogenic cells (OB-CM) or from MNNG/HOS cells (MNNG/HOS-CM). After 24 h, osteogenic cells were washed and maintained for further 24 h, then conditioned media were collected to isolate NPs and perform proteome analysis. Representative dot-plots of gene ontology (GO) enriched terms for (a) biological processes, (b) cellular components and (c) molecular functions. GO processes with the largest LOG (Fold Enrichment) are plotted in order of the LOG (Fold Enrichment). The size of the dots represents the number of proteins in the significant DEPs list associated with the GO term and the color of the dots represent the False Discovery Rate (FDR) values. (d) Representative dot-plot of KEGG enriched pathways. Pathways with the largest LOG (Fold Enrichment) are plotted in order of the LOG (Fold Enrichment). The size of the dots represents the number of proteins in the significant DEPs list associated with the GO term and the color of the dots represent the False Discovery Rate (FDR) values.

from osteogenic cells educated by MNNG/HOS secretome, noteworthy is Angiopoietin-like protein 2 (Angptl2, *alias* Angiopoietin-related protein 2) which has been identified as a strong promoter of osteosarcoma malignancy and lung pre-metastatic niche formation [28–31], as well as L-lactate-dehydrogenase B chain (LdhB), a glycolytic enzyme highly expressed in osteosarcoma cells and associated with poor prognosis [32,33]. Other upregulated proteins, such as Fructose-bisphosphate aldolase A (Aldo A) [34–36], EH domain-containing protein 1 (EHD1) [37,38], follistatin-related protein 1 (Fst-1) [39] and BMP-1 [40] have been implicated in osteosarcoma progression and metastasis and have been proposed as new targets for osteosarcoma treatment [40]. Therefore, this finding suggests the ability of MNNG/HOS cells to fuel their

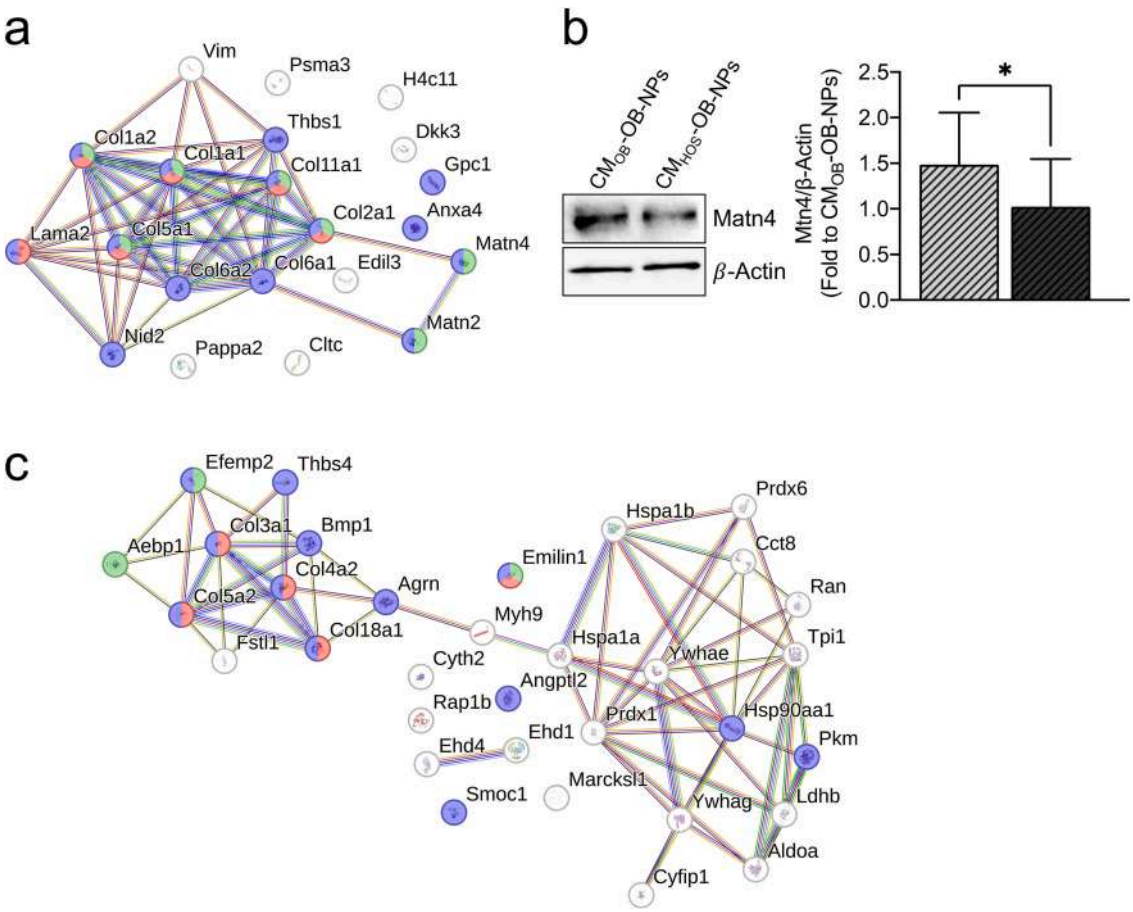

Fig. 7. Protein–Protein Interaction (PPI) network analysis of DEPs between CM_{OB}-OB-NPs and CM_{HOS}-OB-NPs (a) Representative PPI network of the downregulated proteins in CM_{HOS}-OB-NPs, generated by STRING online tool. Nodes represent proteins ($N = 21$), and edges indicate the number of interactions ($N = 128$). Color saturation of the edges represents the confidence score of a functional association. The number of average interactions per node is indicated by the node degree ($N = 4.38$). The clustering coefficient specifies the average node density of the map ($N = 0.439$). Only interactions with a medium confidence score ≥ 0.4 are shown. (b) Western blot and densitometric analysis to evaluate protein expression of Matn4 and β-actin as loading control in protein lysates (10 μg) extracted from CM_{OB}-OB-NPs and CM_{HOS}-OB-NPs. Original uncropped WB with replicates is reported in Supplementary Fig. 7. (c) Representative PPI network of the upregulated proteins in CM_{HOS}-OB-NPs, generated by STRING online tool. Nodes represent proteins ($N = 33$), and edges indicate the number of interactions ($N = 65$). Color saturation of the edges represents the confidence score of a functional association. The number of average interactions per node is indicated by the node degree ($N = 3.94$). The clustering coefficient specifies the average node density of the map ($N = 0.535$). Only interactions with a medium confidence score ≥ 0.4 are shown.

own malignancy by stimulating OB-NPs shuttling of osteosarcoma promoting factors.

Finally, looking at the proteins exclusively expressed in OB-NPs, we obtained some controversial results. In fact, CM_{OB}-OB-NPs protein profile includes Protein deglycase DJ-1, which has been shown to be upregulated in osteosarcoma cells, while its inhibition reduces proliferation and migration and increases apoptosis [41,42]. Nevertheless, Kim et al. demonstrated a physiological role of DJ-1 in osteogenic cells, finding that this protein promotes angiogenesis and osteogenesis by activating FGF receptor-1 signaling [43]. ATP-citrate synthase, another protein uniquely presents in CM_{OB}-OB-NPs, seems to promote osteosarcoma growth and metastasis [44,45]. With regards to the proteins exclusively expressed by OB-NPs educated by MNNG/HOS-CM, again some of them could play a role in osteosarcoma and in osteoblast homeostasis. As an example, it has been found that IGFBP5 restrains osteoblast differentiation by c-Src activation [46], while miR-515-5p/IGF-1R/IGFBP5 axis promotes osteosarcoma cells stemness [47]; Podocan (Podn) has been proposed as a prognostic biomarker correlating with immune infiltrates in osteosarcoma [48]. Septin 2 has been identified in NPs from SAOS-2 osteosarcoma cells and is associated to therapy-related acute myeloid leukemia, a rare complication of osteosarcoma treatment [49]. Fibronectin type III domain-containing protein 1 (Fndc1) promotes bone loss in a postmenopausal osteoporosis mouse model by inhibiting differentiation of bone marrow mesenchymal stem cells [50]. As far as we know, other proteins identified in our proteomic analysis do not seem to have a direct effect on bone homeostasis and/or on bone tumor development, however they could deserve a deeper investigation to identify a possible role in this context. The analysis reveals the absence of a lkaline phosphatase among the proteins identified in both types of OB-NPs. This finding may indicate that certain nanoparticle groups, such as matrix vesicles, are not present in our samples. Alternatively, it could suggest that the sensitivity of the untargeted analysis employed is not adequate for covering all proteins.

Interestingly, recent reports highlight a biological role for NPs in ECM homeostasis and a protein profile reflecting the ECM one. Indeed, Xiao et al. [51] performed a proteomic analysis revealing 83 proteins commonly identified in NPs and in the ECM, including type I collagen, vinculin, α-actinins, thrombospondin-2, vascular cell adhesion protein 1 (V-CAM 1), and periostin. Thouverey et al. [52] found 262 shared proteins between NPs and bone-secreting apical membrane of mineralizing osteoblast-like Saos-2 cells, such as Sphingomyelin phosphodiesterase 3, Inorganic pyrophosphatase 1, Annexin A6, Annexin A2, Integrin β5. Moreover, they observed an enrichment of osteonectin and collagens in EVs, likely playing a role in ECM organization and mineral matrix integrity. Accordingly, selective depletion of annexin A5 or tissue non-specific alkaline phosphatase in NPs impairs calcium deposition and

ECM mineralization [53]. It has been also demonstrated that collagens type VI and XI are electively packaged into NPs, eventually contributing to ECM assembly [54]. Schmidt et al. [55] demonstrated that glycosaminoglycans (GAGs) strongly regulated NPs proteome much more than the cellular proteome, sorting in NPs thrombospondin-1 and -2, fibrillin-1, latent transforming growth factor β-binding protein 2 and cysteine-rich protein 6. Sulphated GAGs presence increases protein composition and sorting in NPs, leading to stronger extracellular matrix formation and mineralization. Finally, Martins et al. [56] reported that osteopontin shuttled in EVs derived from mesenchymal stem cells impact on periodontal ECM by affecting osteoblast and osteoclast function.

In conclusion, our results put one more piece in the intricated puzzle of the vicious cycle between osteosarcoma and bone, dissecting the role of the osteosarcoma secretome and the modification exerted on osteoblast homeostasis and bone matrix organization, eventually promoting osteosarcoma progression and metastasis.

Supplementary data to this article can be found online at https://doi.org/10.1016/j.lfs.2025.123837.

CRediT authorship contribution statement

Argia Ucci: Methodology, Investigation, Data curation. **Luca Giacchi:** Visualization, Methodology, Investigation, Formal analysis. **Maria Concetta Cufaro:** Methodology, Investigation, Formal analysis, Data curation. **Chiara Puri:** Methodology, Investigation. **Michela Ciocca:** Methodology, Investigation. **Fabio Di Ferdinando:** Methodology, Investigation, Data curation. **Piero Del Boccio:** Supervision, Methodology, Investigation, Formal analysis, Data curation. **Alfredo Cappariello:** Writing – review & editing, Validation, Formal analysis, Data curation, Conceptualization. **Nadia Rucci:** Writing – review & editing, Writing – original draft, Validation, Supervision, Resources, Project administration, Funding acquisition, Formal analysis.

Ethics approval

All procedures involving animals and their care were conducted in line with the principles of the Declaration of Helsinki and in conformity with national and international laws and policies (European Economic Community Council Directive 86/609, OJ L 358, 106 1, December 12, 1987; Italian Legislative Decree no. 26, Gazzetta Ufficiale della Repubblica Italiana 107 no. 61, March 4th, 2014; guide for the Care and Use of Laboratory Animals, National Institute of 108 Health, Publication no. 85-23, 1985) and the Animal Research: Reporting of *in Vivo* Experiments (ARRIVE) guidelines. Animal procedures received Institutional approval by the Italian Ministry of Health (approval no. 622/2021-PR).

Funding sources

This work was supported by the Associazione Italiana per la Ricerca sul Cancro (AIRC) Investigator Grant #24823 to NR.

Declaration of competing interest

Nadia Rucci reports financial support was provided by Associazione Italiana per la Ricerca sul Cancro (AIRC, #24823). If there are other authors, they declare that they have no known competing financial interests or personal relationships that could have appeared to influence the work reported in this paper.

Data availability

The authors ensure the availability of supporting data and materials. The datasets analyzed for this study are integrally available upon request.

References

[1] L. Mirabello, R.J. Troisi, S.A. Savage, Osteosarcoma incidence and survival rates from 1973 to 2004: data from the surveillance, epidemiology, and end results program, Cancer 115 (2009) 1531–1543, https://doi.org/10.1002/cncr.24121.
[2] R.L. Siegel, K.D. Miller, H.E. Fuchs, A. Jemal, Cancer statistics, CA Cancer J. Clin. 72 (2022) 7–33, https://doi.org/10.3322/caac.21708.
[3] P.S. Meltzer, L.J. Helman, New horizons in the treatment of osteosarcoma, N. Engl. J. Med. 385 (2021) 2066–2076, https://doi.org/10.1056/NEJMra2103423.
[4] R.A. Durfee, M. Mohammed, H.H. Luu, Review of osteosarcoma and current management, Rheumatol Ther 3 (2016) 221–243, https://doi.org/10.1007/s40744-016-0046-y.
[5] C. Yang, Y. Tian, F. Zhao, Z. Chen, P. Su, Y. Li, A. Qian, Bone microenvironment and osteosarcoma metastasis, Int. J. Mol. Sci. 21 (2020) 6985, https://doi.org/10.3390/ijms21196985.
[6] J. Cui, D. Dean, F.J. Hornicek, Z. Chen, Z. Duan, The role of extracellular matrix in osteosarcoma progression and metastasis, J. Exp. Clin. Cancer Res. 39 (2009) 178, https://doi.org/10.1186/s13046-020-01685-w.
[7] C. Zandueta, C. Ormazábal, N. Perurena, S. Martínez-Canarias, M. Zalacaín, M. San Julián, A.E. Grigoriadis, K. Valencia, F.J. Campos-Laborie, Rivas J. De Las, S. Vicent, A. Patiño-García, F. Lecanda, Matrix-Gla protein promotes osteosarcoma lung metastasis and associates with poor prognosis, J. Pathol. 239 (2016) 438–449, https://doi.org/10.1002/path.4740.
[8] Z. Kun-Peng, Z. Chun-Lin, M. Xiao-Long, Z. Lei, Fibronectin-1 modulated by the long noncoding RNA OIP5-AS1/miR-200b-3p axis contributes to doxorubicin resistance of osteosarcoma cells, J. Cell. Physiol. 234 (2019) 6927–6939, https://doi.org/10.1002/jcp.27435.
[9] F. Jenner, I. Ribitsch, Secretome, extracellular vesicles, exosomes, Orthobiologics (2022) 155–166, https://doi.org/10.1007/978-3-030-84744-9_12.
[10] A. Ucci, A. Cappariello, M. Ponzetti, F. Tennant, A.E.P. Loftus, K. Shefferd, A. Maurizi, S. Delle Monache, A. Teti, N. Rucci, Anti-osteoblastogenic, pro-inflammatory and pro-angiogenic effect of extracellular vesicles isolated from the human osteosarcoma cell line MNNG/HOS, Bone 153 (2021) 116130, https://doi.org/10.1016/j.bone.2021.116130.
[11] M. Ponzetti, A. Ucci, C. Puri, L. Giacchi, I. Flati, D. Capece, F. Zazzeroni, A. Cappariello, N. Rucci, S. Falone, Effects of osteoblast-derived extracellular vesicles on aggressiveness, redox status and mitochondrial bioenergetics of MNNG/HOS osteosarcoma cells, Front. Oncol. 12 (2022) 983254, https://doi.org/10.3389/fonc.2022.983254.
[12] N. Rucci, M. Capulli, S.G. Piperni, A. Cappariello, P. Lau, P. Frings-Meuthen, M. Heer, A. Teti, Lipocalin 2: a new mechanoresponding gene regulating bone homeostasis, J. Bone Miner. Res. 30 (2015) 357–368, https://doi.org/10.1002/jbmr.2341.
[13] N. Rucci, A. Rufo, M. Alamanou, A. Teti, Modeled microgravity stimulates osteoclastogenesis and bone resorption by increasing osteoblast RANKL/OPG ratio, J. Cell. Biochem. 100 (2007) 464–473, https://doi.org/10.1002/jcb.21059.
[14] S. Kruger, Z.Y. Abd-Elmageed, D.H. Hawke, P.M. Wörner, D.A. Jansen, A.B. Abdel-Mageed, E.U. Alt, R. Izadpanah, Molecular characterization of exosome-like vesicles from breast cancer cells, BMC Cancer 14 (2014) 44. http://www.biomedcentral.com/1471-2407/14/44.
[15] K.W. Witwer, E.I. Buzás, L.T. Bemis, A. Bora, C. Lässer, J. Lötvall, E.N. Nolte-'t Hoen, M.G. Piper, S. Sivaraman, J. Skog, C. Théry, M.H. Wauben, F. Hochberg, Standardization of sample collection, isolation and analysis methods in extracellular vesicle research, J Extracell Vesicles. May 27 (2013) 2, https://doi.org/10.3402/jev.v2i0.20360.
[16] J. Kang, D. Liu, Extracellular vesicle isolation methods, in: Z. Li (Ed.), Extracellular Vesicle: Biology and Translational Application, Springer, Singapore, 2024, https://doi.org/10.1007/978-981-97-5536-3_4.
[17] F. Potenza, M.C. Cufaro, L. Di Biase, V. Panella, A. Di Campli, A.G. Ruggieri, B. Dufrusine, E. Restelli, L. Pietrangelo, F. Protasi, D. Pieragostino, V. De Laurenzi, L. Federici, R. Chiesa, M. Sallese, Proteomic analysis of Marinesco–Sjogren syndrome fibroblasts indicates pro-survival metabolic adaptation to SIL1 loss, Int. J. Mol. Sci. 22 (2021) 12449, https://doi.org/10.3390/ijms222212449.
[18] C. Paul, R. Tang, C. Longobardi, R. Lattanzio, T. Eguether, H. Turali, J. Bremond, C. Maurizy, M. Gabola, S. Poupeau, A. Turtoi, E. Denicolai, M.C. Cufaro, M. Svrcek, P. Seksik, V. Castronovo, P. Delvenne, V. de Laurenzi, Q. Da Costa, F. Bertucci, B. Lemmers, D. Pieragostino, E. Mamessier, C. Janke, V. Pinet, M. Hahne, Loss of primary cilia promotes inflammation and carcinogenesis, EMBO Rep. 23 (2022) e55687, https://doi.org/10.15252/embr.202255687.
[19] Wei Fr, Ch. Gao, Wang Jy, Yang Yt, F. Shi, B. Zheng, Label-free quantitative proteomic analysis of three strains of viscerotropic Leishmania isolated from patients with different epidemiological types of visceral Leishmaniasis in China, Acta Parasit 66 (2021) 1366–1386, https://doi.org/10.1007/s11686-021-00387-3.
[20] D. Mendoza-Villanueva, L. Zeef, P. Shore, Metastatic breast cancer cells inhibit osteoblast differentiation through the Runx2/CBFβ-dependent expression of the Wnt antagonist, sclerostin, Breast Cancer Res. 13 (5) (2011) R106, https://doi.org/10.1186/bcr3048.
[21] D.K. Kim, G. Bandara, Y.E. Cho, H.D. Komarow, D.R. Donahue, B. Karim, M. C. Baek, H.M. Kim, D.D. Metcalfe, A. Olivera, Mastocytosis-derived extracellular vesicles deliver miR-23a and miR-30a into pre-osteogenic cells and prevent osteoblastogenesis and bone formation, Nat. Commun. 12 (1) (2021) 2527, https://doi.org/10.1038/s41467-021-22754-4.
[22] A. Cmoch, P. Podszywalow-Bartnicka, M. Palczewska, K. Piwocka, P. Groves, S. Pikula, Stimulators of mineralization limit the invasive phenotype of human osteosarcoma cells by a mechanism involving impaired invadopodia formation, PloS One 9 (2014) e109938, https://doi.org/10.1371/journal.pone.0109938.

[23] Y. Li, G. Meng, Q.-n. Guo, Changes in genomic imprinting and gene expression associated with transformation in a model of human osteosarcoma, Exp. Mol. Pathol. 84 (2008) 234–239, https://doi.org/10.1016/j.yexmp.2008.03.013.
[24] N. Mizoshiri, T. Shirai, R. Terauchi, S. Tsuchida, Y. Mori, D. Hayashi, et al., The tetraspanin CD81 mediates the growth and metastases of human osteosarcoma, Cell. Oncol. (Dordr.) 42 (2019) 861–871, https://doi.org/10.1007/s13402-019-00472-w.
[25] A.R. Klatt, D.P. Nitsche, B. Kobbe, M. Macht, M. Paulsson, R. Wagener, Molecular structure, processing, and tissue distribution of Matrilin-4, J. Biol. Chem. 276 (2001) 17267–17275, https://doi.org/10.1074/jbc.M100587200.
[26] F. Deak, R. Wagener, I. Kiss, M. Paulsson, The matrilins: a novel family of oligomeric extracellular matrix proteins, Matrix Biol. 18 (1999) 55–64, https://doi.org/10.1016/S0945-053X(98)00006-7.
[27] S. Frank, T. Schulthess, R. Landwehr, A. Lustig, T. Mini, P. Jenö, J. Engel, R. A. Kammerer, Characterization of the matrilin coiled-coil domains reveals seven novel isoforms, J. Biol. Chem. 277 (2002) 19071–19079, https://doi.org/10.1074/jbc.M202146200.
[28] B.A. Teicher, Searching for molecular targets in sarcoma, Biochem. Pharmacol. 84 (2012) 1–10, https://doi.org/10.1016/j.bcp.2012.02.009.
[29] H. Odagiri, T. Kadomatsu, M. Endo, T. Masuda, M.S. Morioka, S. Fukuhara, T. Miyamoto, E. Kobayashi, K. Miyata, J. Aoi, H. Horiguchi, N. Nishimura, K. Terada, T. Yakushiji, I. Manabe, N. Mochizuki, H. Mizuta, Y. Oike, The secreted protein ANGPTL2 promotes metastasis of osteosarcoma cells through integrin α5β1, p38 MAPK, and matrix metalloproteinases, Sci Signal 7 (2014) ra7, https://doi.org/10.1126/scisignal.2004612, 2014.
[30] X. Wang, Z. Hu, Z. Wang, Y. Cui, X. Cui, Angiopoietin-like protein 2 is an important facilitator of tumor proliferation, metastasis, angiogenesis and glycolysis in osteosarcoma, Am. J. Transl. Res. 11 (2019) 6341–6355.
[31] M. Charan, P. Dravid, M. Cam, B. Setty, R.D. Roberts, P.J. Houghton, H. Cam, Tumor secreted ANGPTL2 facilitates recruitment of neutrophils to the lung to promote lung pre-metastatic niche formation and targeting ANGPTL2 signaling affects metastatic disease, Oncotarget 11 (2020) 510–522, https://doi.org/10.18632/oncotarget.27433.
[32] P. Chaiyawat, J. Settakorn, A. Sangsin, P. Teeyakasem, J. Klangjorhor, A. Soongkhaw, D. Pruksakorn, Exploring targeted therapy of osteosarcoma using proteomics data, Onco. Targets. Ther. 10 (2017) 565–577, https://doi.org/10.2147/OTT.S119993.
[33] L. Wang, MiR-141-3p overexpression suppresses the malignancy of osteosarcoma by targeting FUS to degrade LDHB, Biosci. Rep. 40 (2020) BSR20193404, https://doi.org/10.1042/BSR20193404.
[34] X. Chen, T.T. Yang, Y. Zhou, W. Wang, X.C. Qiu, J. Gao, C.X. Li, H. Long, B.A. Ma, Q. Ma, X.Z. Zhang, L.J. Yang, Q.Y. Fan, Proteomic profiling of osteosarcoma cells identifies ALDOA and SULT1A3 as negative survival markers of human osteosarcoma, Mol. Carcinog. 53 (2014) 138–144, https://doi.org/10.1002/mc.21957.
[35] F. Long, X. Cai, W. Luo, L. Chen, K. Li, Role of aldolase A in osteosarcoma progression and metastasis: in vitro and in vivo evidence, Oncol. Rep. 32 (2014) 2031–2037, https://doi.org/10.3892/or.2014.3473.
[36] Y. Shen, J. Xu, X. Pan, Y. Zhang, Y. Weng, D. Zhou, S. He, LncRNA KCNQ1OT1 sponges miR-34c-5p to promote osteosarcoma growth via ALDOA enhanced aerobic glycolysis, Cell Death Dis. 11 (2020) 278, https://doi.org/10.1038/s41419-020-2485-1.
[37] H. Yu, G. Qu, Y. Wang, Bao J.J. MaiW, C. Song, M. Yao, The expression of Eps15 homology domain 1 is negatively correlated with disease-free survival and overall survival of osteosarcoma patients, J. Orthop. Surg. Res. 14 (2019) 103, https://doi.org/10.1186/s13018-019-1137-6.
[38] S. Chakraborty, A.M. Bhat, I. Mushtaq, et al., (2023) EHD1-dependent traffic of IGF-1 receptor to the cell surface is essential for Ewing sarcoma tumorigenesis and metastasis, Commun Biol 6 (2023) 758, https://doi.org/10.1038/s42003-023-05125-1.
[39] Y. Ogiwara, M. Nakagawa, F. Nakatani, Y. Uemura, R. Zhang, C. Kudo-Saito, Blocking FSTL1 boosts NK immunity in treatment of osteosarcoma, Cancer Lett. 537 (2022) 215690, https://doi.org/10.1016/j.canlet.2022.215690.
[40] K. Nakajima, T. Kidani, H. Miura, Molecular profiling of bone remodeling occurring in musculoskeletal tumors, J. Orthop. Res. 39 (2021) 1402–1410, https://doi.org/10.1002/jor.24879.
[41] H. Li, X. Hu, B. Ma, H. Zhang, Effect of Parkinson's disease-relevant protein DJ-1 on cell proliferation, apoptosis, invasion and migration in human osteosarcoma cells, Zhong Nan Da Xue Xue Bao Yi Xue Ban 43 (10) (2018) 1054–1060. Oct 28. Chinese, 10.11817/j.issn.1672-7347.2018.10.003. PMID: 30523224.
[42] Z. Ma, J. Yang, Y. Yang, X. Wang, G. Chen, A. Shi, Y. Lu, S. Jia, X. Kang, L. Lu, Rosmarinic acid exerts an anticancer effect on osteosarcoma cells by inhibiting DJ-1 via regulation of the PTEN-PI3K-Akt signaling pathway, Phytomedicine 68 (2020) 153186, https://doi.org/10.1016/j.phymed.2020.153186.
[43] J.M. Kim, H.I. Shin, S.S. Cha, C.S. Lee, B.S. Hong, S. Lim, H.J. Jang, J. Kim, Y. R. Yang, Y.H. Kim, S. Yun, G. Rijal, W. Lee-Kwon, J.K. Seo, Y.S. Gho, S.H. Ryu, E. M. Hur, P.G. Suh, DJ-1 promotes angiogenesis and osteogenesis by activating FGF receptor-1 signaling, Nature Commun 3 (2012) 1296, https://doi.org/10.1038/ncomms2313.
[44] M. Xin, Z. Qiao, J. Li, J. Liu, S. Song, X. Zhao, P. Miao, T. Tang, L. Wang, W. Liu, X. Yang, K. Dai, G. Huang, miR-22 inhibits tumor growth and metastasis by targeting ATP citrate lyase: evidence in osteosarcoma, prostate cancer, cervical cancer and lung cancer, Oncotarget 12 (2016) 44252–44265, https://doi.org/10.18632/oncotarget.10020.
[45] G. Zhu, Y. Xia, Z. Zhao, A. Li, H. Li, T. Xiao, LncRNA XIST from the bone marrow mesenchymal stem cell derived exosome promotes osteosarcoma growth and metastasis through miR-655/ACLY signal, Cancer Cell Int. 22 (2022) 330, https://doi.org/10.1186/s12935-022-02746-0.
[46] B. Peruzzi, A. Cappariello, A. Del Fattore, N. Rucci, F. De Benedetti, A. Teti, c-Src and IL-6 inhibit osteoblast differentiation and integrate IGFBP5 signalling, Nature Commun 3 (2012) 630, https://doi.org/10.1038/ncomms1651.
[47] P. Shi, Y. Li, Q. Guo, Circular RNA circPIP5K1A contributes to cancer stemness of osteosarcoma by miR-515-5p/YAP axis, J. Transl. Med. 19 (2021) 464, https://doi.org/10.1186/s12967-021-03124-6.
[48] F. Yao, Z.F. Zhu, J. Wen, F.Y. Zhang, Z. Zhang, L.Q. Zhu, G.H. Su, Q.W. Yuan, Y. F. Zhen, X.D. Wang, PODN is a prognostic biomarker and correlated with immune infiltrates in osteosarcoma, Cancer Cell Int. 21 (2021) 381, https://doi.org/10.1186/s12935-021-02086-5.
[49] B. Bielorai, C. Meyer, L. Trakhtenbrot, H. Golan, E. Rozner, N. Amariglio, S. Izraeli, R. Marschalek, A. Toren, Therapy-related acute myeloid leukemia with t(2;11)(q37;q23) after treatment for osteosarcoma, Cancer Genet. Cytogenet. 203 (2010) 288–291, https://doi.org/10.1016/j.cancergencyto.2010.08.002.
[50] Y. Xiao, R. Wei, Z. Yuan, X. Lan, J. Kuang, D. Hu, Y. Song, J. Luo, Rutin suppresses FNDC1 expression in bone marrow mesenchymal stem cells to inhibit postmenopausal osteoporosis, Am. J. Transl. Res. 11 (10) (2019) 6680–6690.
[51] Z. Xiao, C.E. Camalier, K. Nagashima, K.C. Chan, D.A. Lucas, M.J. de la Cruz, M. Gignac, S. Lockett, H.J. Issaq, T.D. Veenstra, T.P. Conrads, G.R. Beck Jr., Analysis of the extracellular matrix vesicle proteome in mineralizing osteogenic cells, J. Cell. Physiol. 210 (2) (2007) 325–335, https://doi.org/10.1002/jcp.20826.
[52] C. Thouverey, A. Malinowska, M. Balcerzak, A. Strzelecka-Kiliszek, R. Buchet, M. Dadlez, S. Pikula, Proteomic characterization of biogenesis and functions of matrix vesicles released from mineralizing human osteoblast-like cells, J. Proteomics 74 (7) (2011) 1123–1134, https://doi.org/10.1016/j.jprot.2011.04.005.
[53] L. Bozycki, J. Mroczek, L. Bessueille, S. Mebarek, R. Buchet, S. Pikula, A. Strzelecka-Kiliszek, Annexins A2, A6 and Fetuin-A affect the process of mineralization in vesicles derived from human osteoblastic hFOB 1.19 and osteosarcoma Saos-2 cells, Int. J. Mol. Sci. 22 (8) (2021) 3993, https://doi.org/10.3390/ijms22083993.
[54] J. Morhayim, J. van de Peppel, J.A. Demmers, G. Kocer, A.L. Nigg, M. van Driel, H. Chiba, J.P. van Leeuwen, Proteomic signatures of extracellular vesicles secreted by nonmineralizing and mineralizing human osteogenic cells and stimulation of tumor cell growth, FASEB J. 29 (1) (2015) 274–285, https://doi.org/10.1096/fj.14-261404.
[55] J.R. Schmidt, S. Kliemt, C. Preissler, S. Moeller, M. von Bergen, U. Hempel, S. Kalkhof, Osteoblast-released matrix vesicles, regulation of activity and composition by sulfated and non-sulfated glycosaminoglycans, Mol. Cell. Proteomics 15 (2) (2016) 558–572, https://doi.org/10.1074/mcp.M115.049718.
[56] M. Martins, D. Ribeiro, A. Martins, R.L. Reis, N.M. Neves, Extracellular vesicles derived from osteogenically induced human bone marrow mesenchymal stem cells can modulate lineage commitment, Stem Cell Rep. 6 (3) (2016) 284–291, https://doi.org/10.1016/j.stemcr.2016.01.001.